Revised Version

DESY 01-042
LU-ITP 2001/08
PSI-PR-01-05
UR-1634

arXiv:hep-ph/0104057 v2 6 Apr 2001

DESY 01-042
LU-ITP 2001/08
PSI-PR-01-05
UR-1634
hep-ph/0104057

Probing anomalous quartic gauge-boson couplings via $e^+e^- \to 4$ fermions $+ \gamma$

A. Denner[1], S. Dittmaier[2†], M. Roth[3] and D. Wackeroth[4]

[1] *Paul Scherrer Institut*
CH-5232 Villigen PSI, Switzerland

[2] *Deutsches Elektronen-Synchrotron DESY,*
D-22603 Hamburg, Germany

[3] *Institut für Theoretische Physik, Universität Leipzig*
D-04109 Leipzig, Germany

[4] *Department of Physics and Astronomy, University of Rochester*
Rochester, NY 14627-0171, USA

Abstract:

All lowest-order amplitudes for $e^+e^- \to 4f\gamma$ are calculated including five anomalous quartic gauge-boson couplings that are allowed by electromagnetic gauge invariance and the custodial $SU(2)_c$ symmetry. Three of these anomalous couplings correspond to the operators $\mathcal{L}_0$, $\mathcal{L}_c$, and $\mathcal{L}_n$ that have been constrained by the LEP collaborations in $WW\gamma$ production. The anomalous couplings are incorporated in the Monte Carlo generator RacoonWW.[‡] Moreover, for the processes $e^+e^- \to 4f\gamma$ RacoonWW is improved upon including leading universal electroweak corrections such as initial-state radiation. The discussion of numerical results illustrates the size of the leading corrections as well as the impact of the anomalous quartic couplings for LEP2 energies and at 500 GeV.

April 2001

[†] Heisenberg fellow of the Deutsche Forschungsgemeinschaft

[‡] RacoonWW can be downloaded from `http://www.hep.psi.ch/racoonww/racoonww.html`

1 Introduction

In recent years, the experiments at LEP and the Tevatron have established the existence of elementary self-interactions among three electroweak gauge bosons, mainly by analysing the reactions $e^+e^- \to W^+W^-$ and $p\bar{p} \to W\gamma + X$. The empirical bounds (see e.g. Ref. [1]) on anomalous triple gauge-boson couplings confirm the Standard-Model (SM) couplings at the level of a few per cent. Recently, the LEP collaborations have started to put also bounds on anomalous quartic gauge-boson couplings (AQGC) upon studying the processes $e^+e^- \to W^+W^-\gamma$, $e^+e^- \to Z\gamma\gamma$, and $e^+e^- \to \nu\bar{\nu}\gamma\gamma$. The OPAL [2], L3 [3] and ALEPH collaborations have already presented first results, which have been combined by the LEPEWWG [4].

The experimental analysis of anomalous triple and quartic gauge-boson couplings requires precise predictions from Monte Carlo generators including these anomalous couplings. In particular, it is necessary to account for the instability of the produced weak bosons, which decay into fermion–antifermion pairs. While several generators including triple gauge-boson couplings in $e^+e^- \to WW \to 4f$ exist for quite a long time [5], up to now no generator has been available that deals with the processes $e^+e^- \to WW(\gamma) \to 4f\gamma$ in the presence of AQGC.[1] As a preliminary solution [2, 3] a reweighting technique was used in existing programs for $e^+e^- \to WW(\gamma) \to 4f\gamma$ in the SM where the SM matrix elements were reweighted with the anomalous effects deduced from the program EEWWG [7] for on-shell WWγ production. The aim of this paper is to improve on this situation by implementing the relevant AQGC in the Monte Carlo generator RacoonWW [8], which is at present the only generator for all processes $e^+e^- \to 4f\gamma$. SM predictions for all $4f\gamma$ final states obtained with this generator were presented in Ref. [9]; further results for specific final states can be found in Refs. [6, 10, 11]. Here we supplement these numerical results by a study of AQGC effects at LEP2 and linear collider energies. Moreover, we include two quartic gauge-boson operators in the analysis that, to the best of our knowledge, have not yet been considered in the literature before.

As a second topic, we improve the RacoonWW predictions for $4f\gamma$ production by including the dominant leading electroweak corrections. In particular, we take into account additional initial-state radiation (ISR) at the leading-logarithmic level in the structure-function approach of Ref. [12], where soft-photon effects are exponentiated and collinear logarithms are included up to order $\mathcal{O}(\alpha^3)$. Leading universal effects originating from the renormalization of the electroweak couplings are included by using the so-called G_μ-input-parameter scheme. The singular part [13] of the Coulomb correction, which is relevant for intermediate W-boson pairs in $e^+e^- \to WW(\gamma) \to 4f\gamma$ near their kinematical threshold, is also taken into account.

The paper is organized as follows. In Section 2 we introduce the relevant AQGC and give the corresponding Feynman rules, which are used in Section 3 to calculate the AQGC contributions to all $e^+e^- \to 4f\gamma$ amplitudes. In Section 4 we improve the tree-level predictions by including leading universal electroweak corrections. Section 5 contains our discussion of numerical results, which illustrate the impact of the leading corrections to the SM predictions as well as the effects of the AQGC. A summary is given in Section 6.

[1] While finishing this paper a version of the Monte Carlo generator WRAP [6] became available that also includes AQGC but uses a different set of operators.

2 Anomalous quartic gauge-boson couplings

Since we consider the class of $e^+e^- \to 4f\gamma$ processes in this paper, we restrict our analysis to anomalous quartic gauge-boson couplings (AQGC) that involve at least one photon. Moreover, we consider only genuine AQGC, i.e. we omit all operators that contribute also to triple gauge-boson couplings, such as the quadrilinear part of the well-known operator $F^{\mu\nu}W^{+,\rho}_{\nu}W^{-}_{\rho\mu}$. Imposing in addition a custodial $SU(2)_c$ invariance [14] to keep the ρ parameter close to 1, we are left with operators of dimension 6 or higher. Following Refs. [7, 15, 16, 17] we consider dimension-6 operators for genuine AQGC that respect local $U(1)_{em}$ invariance and global custodial $SU(2)_c$ invariance. These symmetries reduce the set of such operators to a phenomelogically accessible basis. More general AQGC were discussed in Ref. [18].

In order to construct the relevant AQGC, it is convenient to introduce the triplet of massive gauge bosons

$$\overline{\mathbf{W}}_\mu = \left(\overline{W}^1_\mu, \overline{W}^2_\mu, \overline{W}^3_\mu\right) = \left(\frac{1}{\sqrt{2}}(W^+ + W^-)_\mu, \frac{\mathrm{i}}{\sqrt{2}}(W^+ - W^-)_\mu, \frac{1}{c_w} Z_\mu\right), \tag{2.1}$$

where $W^\pm_\mu$ and Z_μ are the fields of the $W^\pm$ and Z bosons, and the (abelian) field-strength tensors

$$\begin{aligned} F^{\mu\nu} &= \partial^\mu A^\nu - \partial^\nu A^\mu, \\ \overline{W}^{i,\mu\nu} &= \partial^\mu \overline{W}^{i,\nu} - \partial^\nu \overline{W}^{i,\mu}, \end{aligned} \tag{2.2}$$

where A_μ is the photon field. The parameter c_w is the cosine of the electroweak mixing angle. The quartic dimension-6 operators are obtained upon contracting two factors of $\overline{\mathbf{W}}_\mu$ with two field-strength tensors. Under the explained symmetry assumptions there are five independent AQGC operators of dimension 6. We choose the following basis:

$$\begin{aligned} \mathcal{L}_0 &= -\frac{e^2}{16\Lambda^2}\, a_0\, F^{\mu\nu} F_{\mu\nu} \overline{\mathbf{W}}_\alpha \overline{\mathbf{W}}^\alpha, \\ \mathcal{L}_c &= -\frac{e^2}{16\Lambda^2}\, a_c\, F^{\mu\alpha} F_{\mu\beta} \overline{\mathbf{W}}^\beta \overline{\mathbf{W}}_\alpha, \\ \mathcal{L}_n &= -\frac{e^2}{16\Lambda^2}\, a_n\, \varepsilon_{ijk} F^{\mu\nu} \overline{W}^i_{\mu\alpha} \overline{W}^j_\nu \overline{W}^{k,\alpha}, \\ \tilde{\mathcal{L}}_0 &= -\frac{e^2}{16\Lambda^2}\, \tilde{a}_0\, F^{\mu\nu} \tilde{F}_{\mu\nu} \overline{\mathbf{W}}_\alpha \overline{\mathbf{W}}^\alpha, \\ \tilde{\mathcal{L}}_n &= -\frac{e^2}{16\Lambda^2}\, \tilde{a}_n\, \varepsilon_{ijk}\, \tilde{F}^{\mu\nu} \overline{W}^i_{\mu\alpha} \overline{W}^j_\nu \overline{W}^{k,\alpha}, \end{aligned} \tag{2.3}$$

where

$$\tilde{F}_{\mu\nu} = \frac{1}{2}\varepsilon_{\mu\nu\rho\sigma} F^{\rho\sigma} \qquad (\varepsilon^{0123} = +1) \tag{2.4}$$

is the dual electromagnetic field-strength tensor, and e is the electromagnetic coupling. The scale Λ is introduced to keep the coupling constants a_i dimensionless. The operators

$\mathcal{L}_0$ and $\mathcal{L}_{\rm c}$, which were introduced in Ref. [15], conserve the discrete symmetries[2] C, P, and CP, while the others respect only one of these symmetries. The operator $\mathcal{L}_{\rm n}$, which was defined in Refs. [7, 16, 17], conserves only P, but violates C and CP. The P-violating operators $\tilde{\mathcal{L}}_0$ and $\tilde{\mathcal{L}}_{\rm n}$ have to our knowledge not yet been considered in the literature. While $\tilde{\mathcal{L}}_0$ conserves C and violates CP, $\tilde{\mathcal{L}}_{\rm n}$ conserves CP and violates C.

We add some comments on the completeness of the set (2.3) of quartic couplings. At first sight, there are three more P-violating couplings of dimension 6 that can be constructed with the tensor $\varepsilon_{\mu\nu\rho\sigma}$, namely

$$\varepsilon_{ijk}\,\varepsilon_{\mu\nu\rho\sigma}\overline{W}^{i,\mu\alpha}\overline{W}^{j,\nu}\overline{W}^{k,\rho}F^{\sigma}{}_{\alpha}, \qquad \varepsilon_{ijk}\,\varepsilon_{\mu\nu\rho\sigma}\overline{W}^{i,\mu\nu}\overline{W}^{j,\rho}\overline{W}^{k,\alpha}F^{\sigma}{}_{\alpha}, \qquad \varepsilon_{\mu\nu\rho\sigma}F^{\mu\nu}F^{\rho\alpha}\overline{\mathbf{W}}^{\sigma}\overline{\mathbf{W}}_{\alpha}. \tag{2.5}$$

These operators can be reduced to $\tilde{\mathcal{L}}_0$ and $\tilde{\mathcal{L}}_{\rm n}$ by exploiting the Schouten identity

$$g_{\alpha\beta}\varepsilon_{\mu\nu\rho\sigma}+g_{\alpha\mu}\varepsilon_{\nu\rho\sigma\beta}+g_{\alpha\nu}\varepsilon_{\rho\sigma\beta\mu}+g_{\alpha\rho}\varepsilon_{\sigma\beta\mu\nu}+g_{\alpha\sigma}\varepsilon_{\beta\mu\nu\rho}=0, \tag{2.6}$$

which is a consequence of the four-dimensionality of space-time. Moreover, we could have constructed also operators from $\partial_\mu\overline{\mathbf{W}}_\nu$ and $\partial_\nu\overline{\mathbf{W}}_\mu$ separately instead of taking $\overline{\mathbf{W}}_{\mu\nu}$. However, the new operators obtained this way only lead to additional terms involving either $\partial^\mu\overline{\mathbf{W}}_\mu$ or $\partial^\mu F_{\mu\nu}$, which do not contribute to the amplitudes for $\mathrm{e}^+\mathrm{e}^-\to 4f\gamma$ for massless external fermions.

In order to deduce the Feynman rules for the considered AQGC, we express the fields $\overline{W}^i_\mu$ in terms of physical fields,

$$\begin{aligned}
\overline{\mathbf{W}}_\mu\overline{\mathbf{W}}_\nu &= W^+_\mu W^-_\nu + W^-_\mu W^+_\nu + \frac{1}{c_{\rm w}^2}Z_\mu Z_\nu,\\
\varepsilon_{ijk}\overline{W}^{i,\mu\nu}\overline{W}^{j,\rho}\overline{W}^{k,\sigma} &= \frac{\mathrm{i}}{c_{\rm w}}\Big[W^+_{\mu\nu}(W^-_\sigma Z_\rho - W^-_\rho Z_\sigma) - W^-_{\mu\nu}(W^+_\sigma Z_\rho - W^+_\rho Z_\sigma)\\
&\qquad + Z_{\mu\nu}(W^+_\sigma W^-_\rho - W^+_\rho W^-_\sigma)\Big].
\end{aligned} \tag{2.7}$$

Taking all fields and momenta as incoming, we obtain the Feynman rules

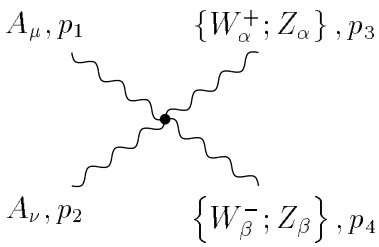

$$= \mathrm{i}\frac{e^2}{8\Lambda^2}\left\{1;\frac{1}{c_{\rm w}^2}\right\}$$

$$\begin{aligned}
&\times\{4\,a_0\,g^{\alpha\beta}[(p_1p_2)g^{\mu\nu}-p_1^\nu p_2^\mu]\\
&\quad + a_{\rm c}\,[(p_1^\alpha p_2^\beta + p_1^\beta p_2^\alpha)g^{\mu\nu} + (p_1p_2)(g^{\mu\alpha}g^{\nu\beta}+g^{\nu\alpha}g^{\mu\beta})
\end{aligned}$$

[2] We adopt the usual convention [19] that $PV_\mu P^{-1}=V^\mu$ and $CV_\mu C^{-1}=-V_\mu^\dagger$ for all electroweak gauge bosons. While for the photon ($V=A$) these transformations follow from the C and P invariance of the electromagnetic interaction, for the weak bosons ($V=W^\pm, Z$) they are mere definitions, which are, however, in agreement with the C and P invariance of the bosonic part of the electroweak interaction. The CP transformation, on the other hand, is well-defined for all electroweak gauge bosons.

$$
\begin{aligned}
&- p_1^\nu (p_2^\beta g^{\mu\alpha} + p_2^\alpha g^{\mu\beta}) - p_2^\mu (p_1^\beta g^{\nu\alpha} + p_1^\alpha g^{\nu\beta})] \\
&+ 4\,\tilde{a}_0\, g^{\alpha\beta} p_{1\rho} p_{2\sigma} \varepsilon^{\mu\rho\nu\sigma}\},
\end{aligned} \tag{2.8}
$$

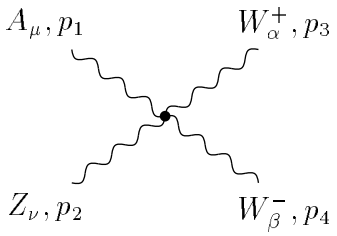

$$
= -\frac{e^2}{16\Lambda^2 c_{\rm w}}
$$

$$
\begin{aligned}
\times\{&a_{\rm n}\,[-(p_1p_2)(g^{\mu\alpha}g^{\beta\nu} - g^{\mu\beta}g^{\nu\alpha}) - (p_1p_3)(g^{\mu\beta}g^{\nu\alpha} - g^{\mu\nu}g^{\alpha\beta}) - (p_1p_4)(g^{\mu\nu}g^{\alpha\beta} - g^{\mu\alpha}g^{\beta\nu}) \\
&+ p_2^\mu (p_1^\alpha g^{\beta\nu} - p_1^\beta g^{\nu\alpha}) + p_3^\mu (p_1^\beta g^{\nu\alpha} - p_1^\nu g^{\alpha\beta}) + p_4^\mu (p_1^\nu g^{\alpha\beta} - p_1^\alpha g^{\beta\nu}) \\
&- g^{\mu\nu}(p_1^\beta p_3^\alpha - p_1^\alpha p_4^\beta) - g^{\mu\alpha}(p_1^\nu p_4^\beta - p_1^\beta p_2^\nu) - g^{\mu\beta}(p_1^\alpha p_2^\nu - p_1^\nu p_3^\alpha)] \\
+\;&\tilde{a}_{\rm n}\, p_{1\rho}[(p_1+p_2)^\nu \varepsilon^{\alpha\beta\mu\rho} + (p_1+p_3)^\alpha \varepsilon^{\beta\nu\mu\rho} + (p_1+p_4)^\beta \varepsilon^{\nu\alpha\mu\rho} \\
&- (p_2-p_3)_\sigma g^{\nu\alpha} \varepsilon^{\sigma\beta\mu\rho} - (p_3-p_4)_\sigma g^{\alpha\beta} \varepsilon^{\sigma\nu\mu\rho} - (p_4-p_2)_\sigma g^{\beta\nu} \varepsilon^{\sigma\alpha\mu\rho}]\}.
\end{aligned} \tag{2.9}
$$

Note that the γZW^+W^- coupling is symmetric with respect to cyclic permutations of ZW^+W^-, i.e. of $(p_2,\nu),(p_3,\alpha),(p_4,\beta)$.

In order to evaluate the diagrams with the P-violating couplings within the Weyl–van der Waerden spinor formalism (see Ref. [20] and references therein), which we use in the calculation of our amplitudes, the tensor $\varepsilon^{\mu\nu\rho\sigma}$ has to be translated into the spinor technique. Following the notation of Ref. [20] the tensor is substituted in the Feynman rules according to the identity ($\varepsilon^{0123} = +1$)

$$
\varepsilon^{\mu\nu\rho\sigma} \left(\tfrac{1}{2}\sigma_\mu^{\dot{A}B}\right)\left(\tfrac{1}{2}\sigma_\nu^{\dot{C}D}\right)\left(\tfrac{1}{2}\sigma_\rho^{\dot{E}F}\right)\left(\tfrac{1}{2}\sigma_\sigma^{\dot{G}H}\right) \;=\; \frac{\mathrm{i}}{4}\left(\epsilon^{\dot{A}\dot{E}}\epsilon^{\dot{C}\dot{G}}\epsilon^{BD}\epsilon^{FH} - \epsilon^{\dot{A}\dot{C}}\epsilon^{\dot{E}\dot{G}}\epsilon^{BF}\epsilon^{DH}\right). \tag{2.10}
$$

For the the Standard-Model (SM) parameters and fields, i.e. for the SM Feynman rules, we follow the conventions of Ref. [21].[3]

3 Amplitudes with anomalous quartic gauge-boson couplings

In Ref. [9] we have presented the SM amplitudes for all $\mathrm{e^+e^-} \to 4f\gamma$ processes with massless fermions in a generic way. The various channels have been classified into charged-current (CC), neutral-current (NC), and mixed CC/NC reactions, and all amplitudes have been generated from the matrix elements $\mathcal{M}_{\rm CCa}$ and $\mathcal{M}_{\rm NCa}$, which correspond to the simplest CC and NC reactions, called CCa and NCa, respectively:

CCa: $\quad \mathrm{e^+e^-} \to f\bar{f}'F\bar{F}'$,

NCa: $\quad \mathrm{e^+e^-} \to f\bar{f}F\bar{F}$,

[3] In this context it is important to recall that different conventions are used in the literature concerning the sign of the electroweak gauge coupling $g \equiv e/s_{\rm w}$, and thus of the sign of the sine of the weak mixing angle $s_{\rm w}$. Since the SM quartic coupling $\gamma\mathrm{ZW^+W^-}$ changes under the inversion of this sign, which of course can never affect physical quantities, the anomalous $\gamma\mathrm{ZW^+W^-}$ coupling also has to be reversed when switching from one convention to the other, although $s_{\rm w}$ does not appear in (2.9) explicitly.

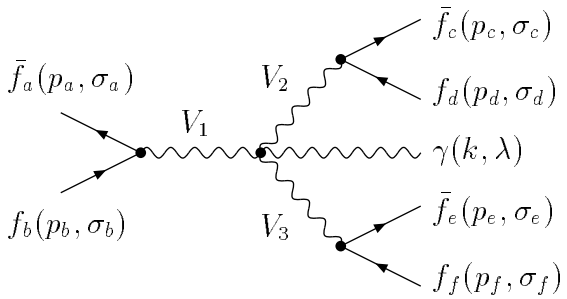

Figure 1: Generic diagram for the AQGC contribution to $\mathrm{e}^+\mathrm{e}^- \to 4f\gamma$

where f and F are different fermions ($f \neq F$) that are neither electrons nor electron neutrinos ($f, F \neq \mathrm{e}^-, \nu_\mathrm{e}$) and their weak-isospin partners are denoted by f' and F', respectively. Here we supplement the SM amplitudes of Ref. [9] by the corresponding contributions resulting from the AQGC given in (2.3). We follow entirely the conventions of Ref. [9] and denote the external particles of the considered reaction according to

$$\mathrm{e}^+(p_+,\sigma_+) + \mathrm{e}^-(p_-,\sigma_-) \to f_1(k_1,\sigma_1) + \bar{f}_2(k_2,\sigma_2) + f_3(k_3,\sigma_3) + \bar{f}_4(k_4,\sigma_4) + \gamma(k_5,\lambda), \tag{3.1}$$

where the momenta and helicities are given in parentheses. We list the expressions for the contributions $\delta\mathcal{M}_{\mathrm{CCa,AQGC}}$ and $\delta\mathcal{M}_{\mathrm{NCa,AQGC}}$ of the anomalous couplings to the generic CC and NC matrix elements $\mathcal{M}_{\mathrm{CCa}}$ and $\mathcal{M}_{\mathrm{NCa}}$, respectively, which have to be added to the SM contributions. From $\mathcal{M}_{\mathrm{CCa}}$ and $\mathcal{M}_{\mathrm{NCa}}$ the amplitudes for all other CC, NC, and CC/NC reactions are constructed as explained in Ref. [9]. Some minor corrections to this generic construction are given in App. A.

We express the AQGC contributions $\delta\mathcal{M}_{\mathrm{CCa,AQGC}}$ and $\delta\mathcal{M}_{\mathrm{NCa,AQGC}}$ in terms of the two generic functions $\mathcal{M}_{\gamma VV,\mathrm{AQGC}}$ and $\mathcal{M}_{ZWW,\mathrm{AQGC}}$, which correspond to the $\gamma\gamma VV$ and γZWW couplings, respectively, with $V = W, Z$,

$$\begin{aligned}
&\delta\mathcal{M}^{\sigma_+,\sigma_-,\sigma_1,\sigma_2,\sigma_3,\sigma_4,\lambda}_{\mathrm{CCa,AQGC}}(p_+,p_-,k_1,k_2,k_3,k_4,k_5)\\
&\quad= \mathcal{M}^{\sigma_+,\sigma_-,-\sigma_1,-\sigma_2,-\sigma_3,-\sigma_4,\lambda}_{\gamma WW,\mathrm{AQGC}}(p_+,p_-,-k_1,-k_2,-k_3,-k_4,k_5)\\
&\qquad+ \mathcal{M}^{\sigma_+,\sigma_-,-\sigma_1,-\sigma_2,-\sigma_3,-\sigma_4,\lambda}_{ZWW,\mathrm{AQGC}}(p_+,p_-,-k_1,-k_2,-k_3,-k_4,k_5),
\end{aligned} \tag{3.2}$$

$$\begin{aligned}
&\delta\mathcal{M}^{\sigma_+,\sigma_-,\sigma_1,\sigma_2,\sigma_3,\sigma_4,\lambda}_{\mathrm{NCa,AQGC}}(p_+,p_-,k_1,k_2,k_3,k_4,k_5)\\
&\quad= \mathcal{M}^{\sigma_+,\sigma_-,-\sigma_1,-\sigma_2,-\sigma_3,-\sigma_4,\lambda}_{\gamma ZZ,\mathrm{AQGC}}(p_+,p_-,-k_1,-k_2,-k_3,-k_4,k_5)\\
&\qquad+ \mathcal{M}^{-\sigma_1,-\sigma_2,-\sigma_3,-\sigma_4,\sigma_+,\sigma_-,\lambda}_{\gamma ZZ,\mathrm{AQGC}}(-k_1,-k_2,-k_3,-k_4,p_+,p_-,k_5)\\
&\qquad+ \mathcal{M}^{-\sigma_3,-\sigma_4,\sigma_+,\sigma_-,-\sigma_1,-\sigma_2,\lambda}_{\gamma ZZ,\mathrm{AQGC}}(-k_3,-k_4,p_+,p_-,-k_1,-k_2,k_5).
\end{aligned} \tag{3.3}$$

The generic Feynman graph that corresponds to $\mathcal{M}_{V_1V_2V_3,\mathrm{AQGC}}$ is shown in Figure 1, where the fermions and antifermions are assumed as incoming and the photon as outgoing. Explicitly the generic functions read

$$\begin{aligned}
&\mathcal{M}^{\sigma_a,\sigma_b,\sigma_c,\sigma_d,\sigma_e,\sigma_f,\lambda}_{\gamma VV,\mathrm{AQGC}}(p_a,p_b,p_c,p_d,p_e,p_f,k)\\
&\quad= -\frac{e^5 C_{\gamma\gamma VV}}{8\sqrt{2}\Lambda^2}\delta_{\sigma_a,-\sigma_b}\delta_{\sigma_c,-\sigma_d}\delta_{\sigma_e,-\sigma_f}\, g^{\sigma_b}_{\gamma\bar{f}_a f_b} g^{\sigma_d}_{V\bar{f}_c f_d} g^{\sigma_f}_{V\bar{f}_e f_f} P_V(p_c+p_d) P_V(p_e+p_f)
\end{aligned}$$

$$\times \Big[8 A_{a_0}^{\sigma_a,\sigma_c,\sigma_e,\lambda}(p_a,p_b,p_c,p_d,p_e,p_f,k) + A_{a_c}^{\sigma_a,\sigma_c,\sigma_e,\lambda}(p_a,p_b,p_c,p_d,p_e,p_f,k) \Big],$$

$$\text{with} \quad C_{\gamma\gamma ZZ} = 1/c_{\rm w}^2, \quad C_{\gamma\gamma WW} = 1, \tag{3.4}$$

$$\begin{aligned}
&\mathcal{M}_{ZWW,\mathrm{AQGC}}^{\sigma_a,\sigma_b,\sigma_c,\sigma_d,\sigma_e,\sigma_f,\lambda}(p_a,p_b,p_c,p_d,p_e,p_f,k) \\
&\quad = \frac{\mathrm{i}e^5}{8\sqrt{2}c_{\rm w}\Lambda^2}\delta_{\sigma_a,-\sigma_b}\delta_{\sigma_c,+}\delta_{\sigma_d,-}\delta_{\sigma_e,+}\delta_{\sigma_f,-}\,(Q_c-Q_d) g_{Z\bar f_a f_b}^{\sigma_b} g_{\bar W \bar f_c f_d} g_{\bar W \bar f_e f_f} \\
&\qquad \times P_Z(p_a+p_b) P_W(p_c+p_d) P_W(p_e+p_f)\, A_{a_{\rm n}}^{\sigma_a,\sigma_c,\sigma_e,\lambda}(p_a,p_b,p_c,p_d,p_e,p_f,k),
\end{aligned} \tag{3.5}$$

where the propagator functions $P_V(p)$ and the fermion–gauge-boson couplings $g_{V\bar f f'}^{\sigma}$ can be found in Ref. [9]. We have evaluated the auxiliary functions $A_{a_k}^{\sigma_a,\sigma_c,\sigma_d,\lambda}$ with $k = 0, \mathrm{c}, \mathrm{n}$ in terms of Weyl–van der Waerden spinor products [20]:

$$A_{a_0}^{++++}(p_a,p_b,p_c,p_d,p_e,p_f,k) = (a_0 + \mathrm{i}\tilde a_0)\,\frac{(\langle p_b k\rangle^*)^2\,\langle p_d p_f\rangle^* \langle p_c p_e\rangle}{\langle p_a p_b\rangle^*}, \tag{3.6}$$

$$\begin{aligned}
&A_{a_c}^{++++}(p_a,p_b,p_c,p_d,p_e,p_f,k) = \frac{a_{\rm c}}{(p_a\cdot p_b)} \\
&\times \Big[2\langle p_a p_b\rangle^* \langle p_d k\rangle^* \langle p_f k\rangle^* \langle p_a p_c\rangle \langle p_a p_e\rangle + (\langle p_b k\rangle^*)^2\,\langle p_d p_f\rangle^* \langle p_a p_b\rangle \langle p_c p_e\rangle \Big],
\end{aligned} \tag{3.7}$$

$$\begin{aligned}
&A_{a_{\rm n}}^{++++}(p_a,p_b,p_c,p_d,p_e,p_f,k) = (a_{\rm n} + \mathrm{i}\tilde a_{\rm n}) \\
&\times \Big\{ \quad \langle p_b p_f\rangle^* \langle p_d k\rangle^* \langle p_a p_e\rangle \Big[\langle p_a k\rangle^* \langle p_a p_c\rangle + \langle p_b k\rangle^* \langle p_b p_c\rangle + \langle p_e k\rangle^* \langle p_c p_e\rangle + \langle p_f k\rangle^* \langle p_c p_f\rangle \Big] \\
&\quad + \langle p_b p_d\rangle^* \langle p_f k\rangle^* \langle p_a p_c\rangle \Big[\langle p_c k\rangle^* \langle p_c p_e\rangle + \langle p_d k\rangle^* \langle p_d p_e\rangle - \langle p_a k\rangle^* \langle p_a p_e\rangle - \langle p_b k\rangle^* \langle p_b p_e\rangle \Big] \\
&\quad - \langle p_d p_f\rangle^* \langle p_b k\rangle^* \langle p_c p_e\rangle \Big[\langle p_e k\rangle^* \langle p_a p_e\rangle + \langle p_f k\rangle^* \langle p_a p_f\rangle - \langle p_c k\rangle^* \langle p_a p_c\rangle - \langle p_d k\rangle^* \langle p_a p_d\rangle \Big] \Big\}.
\end{aligned} \tag{3.8}$$

The remaining polarization combinations follow from crossing and discrete symmetries,

$$\begin{aligned}
A_{a_k}^{++-+}(p_a,p_b,p_c,p_d,p_e,p_f,k) &= A_{a_k}^{++++}(p_a,p_b,p_c,p_d,p_f,p_e,k), \\
A_{a_k}^{+-++}(p_a,p_b,p_c,p_d,p_e,p_f,k) &= A_{a_k}^{++++}(p_a,p_b,p_d,p_c,p_e,p_f,k), \\
A_{a_k}^{+--+}(p_a,p_b,p_c,p_d,p_e,p_f,k) &= A_{a_k}^{++++}(p_a,p_b,p_d,p_c,p_f,p_e,k), \\
A_{a_k}^{-+++}(p_a,p_b,p_c,p_d,p_e,p_f,k) &= A_{a_k}^{++++}(p_b,p_a,p_c,p_d,p_e,p_f,k), \\
A_{a_k}^{-++-}(p_a,p_b,p_c,p_d,p_e,p_f,k) &= A_{a_k}^{++++}(p_b,p_a,p_c,p_d,p_f,p_e,k), \\
A_{a_k}^{--++}(p_a,p_b,p_c,p_d,p_e,p_f,k) &= A_{a_k}^{++++}(p_b,p_a,p_d,p_c,p_e,p_f,k), \\
A_{a_k}^{---+}(p_a,p_b,p_c,p_d,p_e,p_f,k) &= A_{a_k}^{++++}(p_b,p_a,p_d,p_c,p_f,p_e,k), \\
A_{a_k}^{\sigma_a,\sigma_c,\sigma_d,-}(p_a,p_b,p_c,p_d,p_e,p_f,k) &= \Big(A_{a_k}^{-\sigma_a,-\sigma_c,-\sigma_d,+}(p_a,p_b,p_c,p_d,p_e,p_f,k)\Big)^*, \quad k = 0,\mathrm{c},\mathrm{n}.
\end{aligned} \tag{3.9}$$

It is interesting to observe that the helicity amplitudes for a_0 and $\tilde a_0$, and similarly for $a_{\rm n}$ and $\tilde a_{\rm n}$, differ only in factors $\pm\mathrm{i}$ for equal coupling factors. These AQGC are the ones that are related by interchanging a field-strength tensor F with a dual field-strength tensor $\tilde F$ in the corresponding operators in (2.3).

As we had already done in Ref. [9] in the case of the SM amplitudes, we have numerically checked the amplitudes with the AQGC against an evaluation by *Madgraph* [22],

which we have extended by the anomalous couplings. We find numerical agreement for a set of representative $4f\gamma$ final states.

4 Leading universal electroweak corrections

Besides the genuine AQGC we have also included the dominant leading electroweak corrections to $e^+e^- \to 4f\gamma$ into RacoonWW, similar to our construction [23] of an improved Born approximation (IBA) for $e^+e^- \to WW \to 4f$.

The dominant universal effects originating from the renormalization of the electroweak couplings are included by using the so-called G_μ-input-parameter scheme. To this end, the global factor α^5 in the cross section is replaced by $\alpha_{G_\mu}^4 \alpha(0)$ with

$$\alpha_{G_\mu} = \frac{\sqrt{2} G_\mu M_W^2 s_w^2}{\pi}. \tag{4.1}$$

While the fine-structure constant $\alpha(0)$ yields the correct coupling for the external on-shell photon, α_{G_μ} takes into account the running of the electromagnetic coupling from zero to M_W^2 and the leading universal m_t-dependent corrections to CC processes correctly. The m_t-dependent correction to NC processes are not included completely. These could be accounted for by introducing an appropriate effective weak mixing angle. However, we prefer to keep the weak mixing angle fixed by $c_w^2 = 1 - s_w^2 = M_W^2/M_Z^2$, in order to avoid potential problems with gauge invariance which may result by violating this condition.

Initial-state radiation (ISR) to $e^+e^- \to 4f\gamma$ is implemented at the leading-logarithmic level in the structure-function approach of Ref. [12] as described for $e^+e^- \to 4f$ in Ref. [8] in equations (5.1)–(5.4),

$$\int \mathrm{d}\sigma_{\mathrm{IBA}}^{e^+e^- \to 4f\gamma} = \int_0^1 \mathrm{d}x_1 \int_0^1 \mathrm{d}x_2 \, \Gamma_{ee}^{\mathrm{LL}}(x_1, Q^2) \Gamma_{ee}^{\mathrm{LL}}(x_2, Q^2) \int \mathrm{d}\hat{\sigma}_{\mathrm{IBA}}^{e^+e^- \to 4f\gamma}(x_1 p_+, x_2 p_-). \tag{4.2}$$

In the structure function $\Gamma_{ee}^{\mathrm{LL}}(x, Q^2)$ [8, 24] soft-photon effects are exponentiated and collinear logarithms are included up to order $\mathcal{O}(\alpha^3)$. The QED splitting scale Q^2 is a free parameter in leading-logarithmic approximation and has to be set to a typical momentum scale of the process. It is fixed as $Q^2 = s$ by default but can be changed to any other scale in order to adjust the IBA to the full correction or to estimate the intrinsic uncertainty of the IBA by choosing different values for Q^2.

For processes with intermediate W-boson pairs, $e^+e^- \to WW(\gamma) \to 4f\gamma$, the singular part [13] of the Coulomb correction is taken into account, i.e. in this case we have

$$\mathrm{d}\hat{\sigma}_{\mathrm{IBA}}^{e^+e^- \to 4f\gamma} = \mathrm{d}\hat{\sigma}_{\mathrm{Born}}^{e^+e^- \to 4f\gamma} \left[1 + \delta_{\mathrm{Coul}}(s', k_+^2, k_-^2) g(\bar{\beta})\right], \qquad s' = (k_+ + k_-)^2. \tag{4.3}$$

The Coulomb singularity arises from diagrams where a soft photon is exchanged between two nearly on-shell W bosons close to their kinematical production threshold and results in a simple factor that depends on the momenta $k_\pm$ of the W bosons [13, 25],

$$\delta_{\mathrm{Coul}}(s', k_+^2, k_-^2) = \frac{\alpha(0)}{\bar{\beta}} \mathrm{Im} \left\{ \ln \left(\frac{\beta - \bar{\beta} + \Delta_M}{\beta + \bar{\beta} + \Delta_M} \right) \right\},$$

$$\bar{\beta} = \frac{\sqrt{s'^2 + k_+^4 + k_-^4 - 2s'k_+^2 - 2s'k_-^2 - 2k_+^2 k_-^2}}{s'},$$

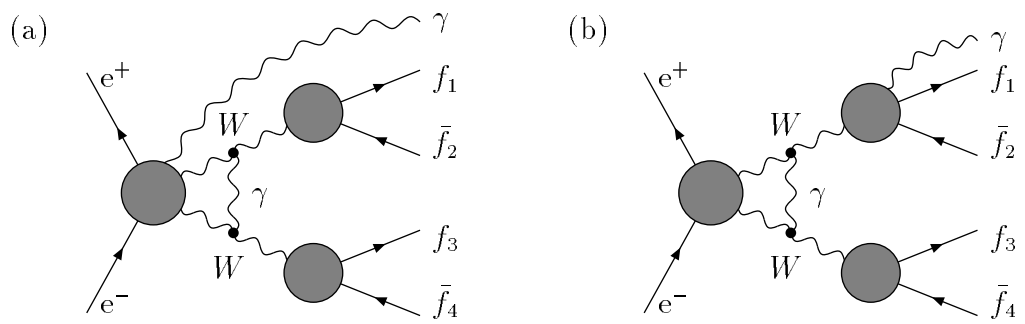

Figure 2: Generic diagrams contributing to the Coulomb singularity in $e^+e^- \to 4f\gamma$

$$\beta = \sqrt{1 - \frac{4(M_W^2 - iM_W\Gamma_W)}{s'}}, \qquad \Delta_M = \frac{|k_+^2 - k_-^2|}{s'}. \tag{4.4}$$

This correction factor is multiplied with the auxiliary function

$$g(\bar{\beta}) = \left(1 - \bar{\beta}^2\right)^2, \tag{4.5}$$

in order to restrict the impact of δ_{Coul} to the threshold region where it is valid.

For $e^+e^- \to 4f\gamma$ both diagrams where the real photon is emitted from the initial state (see Figure 2a) or from the final state (see Figure 2b) contribute to the Coulomb singularity. Therefore, it is not just given by a factor to the complete matrix element. However, applying different correction factors to different diagrams would violate gauge invariance. Therefore, we decided to use an effective treatment that takes into account the dominant effects of the Coulomb singularity. We actually implemented two different variants:

1. In the first variant we multiply the complete matrix element with the Coulomb correction factor with $k_+ = k_1 + k_2$ and $k_- = k_3 + k_4$. In this way we multiply the correct Coulomb correction to all diagrams with ISR (Figure 2a). However, in this approach we do not treat the Coulomb singularity in diagrams with final-state radiation (Figure 2b) properly. Nevertheless, this recipe should yield a good description of the Coulomb singularity, since the diagrams with two resonant W bosons and photon emission from the initial state dominate the cross section. This expectation is confirmed by the numerical results presented below.

2. In the second variant we improve on this prescription by differentiating between initial-state and final-state radiation according to the invariant masses in the final state. To this end, the W-boson momenta entering the Coulomb correction factor are fixed as

$$(k_+, k_-) = \begin{cases} (k_1 + k_2, k_3 + k_4) & \text{for } \Delta_{12} < \Delta_{125}, \Delta_{34} < \Delta_{345}, \\ (k_1 + k_2 + k_5, k_3 + k_4) & \text{for } \Delta_{12} > \Delta_{125}, \Delta_{34} < \Delta_{345} \quad \text{or} \\ & \Delta_{12} > \Delta_{125}, \Delta_{34} > \Delta_{345}, \Delta_{125} < \Delta_{345}, \\ (k_1 + k_2, k_3 + k_4 + k_5) & \text{for } \Delta_{12} < \Delta_{125}, \Delta_{34} > \Delta_{345} \quad \text{or} \\ & \Delta_{12} > \Delta_{125}, \Delta_{34} > \Delta_{345}, \Delta_{125} > \Delta_{345}, \end{cases} \tag{4.6}$$

where $\Delta_{ij} = |(k_i + k_j)^2 - M_W^2|$ and $\Delta_{ijl} = |(k_i + k_j + k_l)^2 - M_W^2|$. In this way we effectively apply the correct Coulomb correction factor to all dominating doubly-resonant contributions, shown in Figure 2.

The Coulomb singularity is not included in processes that do not involve diagrams with two resonant W bosons.

Finally, we optionally include the naive QCD correction factors $(1 + \alpha_s/\pi)$ for each hadronically decaying W boson.

In order to avoid any kind of mismatch with the decay, Γ_W is calculated in lowest order using the G_μ scheme. This choice guarantees that the "effective branching ratios", which result after integrating out the decay parts, add up to one when summing over all channels. Of course, if naive QCD corrections are taken into account, these are also included in the calculation of the total W-boson width.

5 Numerical results

For our numerical analysis we take the same SM input parameters as in Refs. [8, 11]. We use the constant-width scheme, which has been shown to be practically equivalent to the complex-mass scheme for the considered processes in Ref. [9]. The errorbars shown in the plots for the relative corrections result from the statistical errors of the Monte-Carlo integration.

5.1 Comparison with existing results

We first compare our results for $e^+e^- \to 4f\gamma$ including leading corrections with results existing in the literature.

Predictions for $e^+e^- \to 4f\gamma$ including ISR corrections have been provided with the program WRAP [6]. First results have been published in Ref. [11] where also a comparison with RacoonWW at tree level was performed. Here we present a comparison between WRAP and RacoonWW for the same set of input parameters and cuts as in Section 5.2. of Ref. [11] but including ISR. In this tuned comparison, the W-boson width is kept fixed at $\Gamma_W = 2.04277\,\mathrm{GeV}$, and neither the Coulomb singularity nor naive QCD corrections are included. The results are shown in Figures 3 and 4. The absolute predictions on the left-hand sides are hardly distinguishable. The relative deviations shown on the right-hand sides reveal that the agreement between WRAP and RacoonWW is at the level of the statistical error of about 0.2%. The comparison has been made for collinear structure functions. Unlike p_T-dependent structure functions, collinear structure functions do not allow to take into account the Bose symmetry of the final-state photons resulting in some double counting [26]. However, for not too small cuts on the photon energy and angle these effects are beyond the accuracy of the leading-logarithmic approximation. This has been confirmed by the numerical analysis in Ref. [6].

In Figures 5–7 we repeat the comparison between YFSWW3-1.14 (scheme A) [27] and RacoonWW given in Section 4.1. of Ref. [11] for the photonic distributions. But now we include besides the tree-level predictions of RacoonWW for $e^+e^- \to 4f\gamma$ also those including leading-logarithmic ISR. Note that unlike in all other distributions discussed here, a recombination of photons with fermions is performed for this comparison.

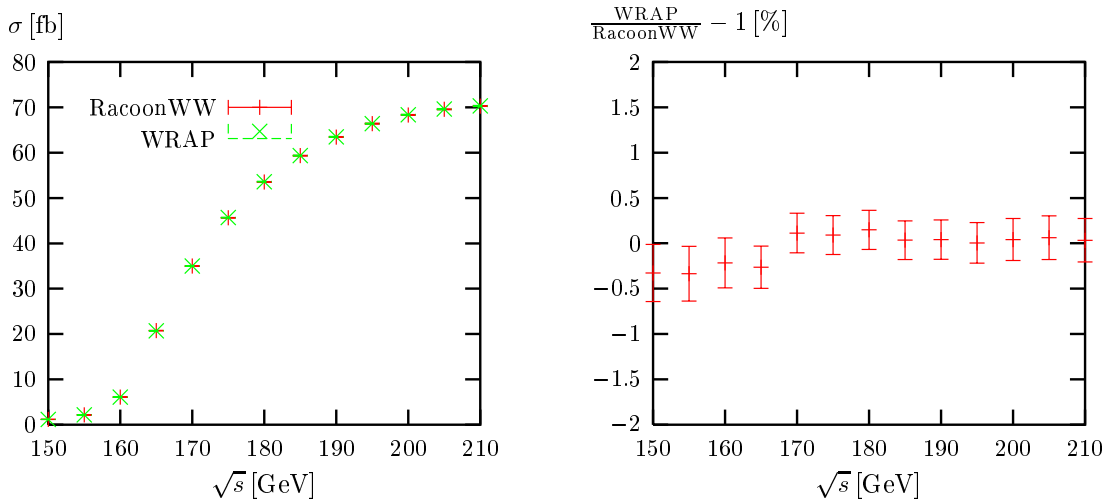

Figure 3: Total cross section including leading-logarithmic ISR corrections for the process $e^+e^- \to u\bar{d}\mu^-\bar{\nu}_\mu\gamma$ as a function of the CM energy with minimal energy of the observed photon of 1 GeV. Absolute predictions from WRAP [6] and RacoonWW are shown on the left-hand side, the relative differences between the two programs are shown on the right-hand side.

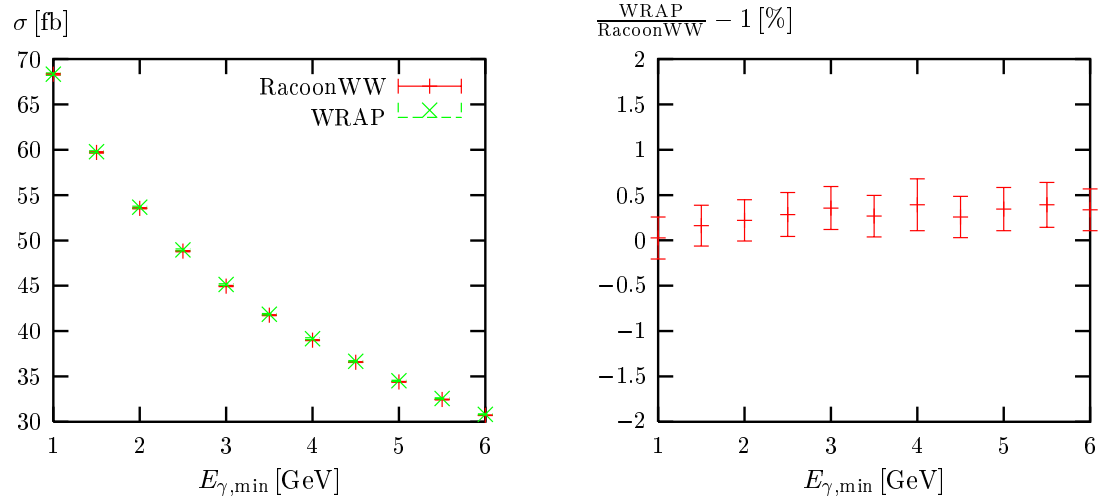

Figure 4: Total cross section including leading-logarithmic ISR corrections for the process $e^+e^- \to u\bar{d}\mu^-\bar{\nu}_\mu\gamma$ as a function of the minimal energy of the observed photon for $\sqrt{s} = 192$ GeV. Absolute predictions from WRAP [6] and RacoonWW are shown on the left-hand side, the relative differences between the two programs are shown on the right-hand side.

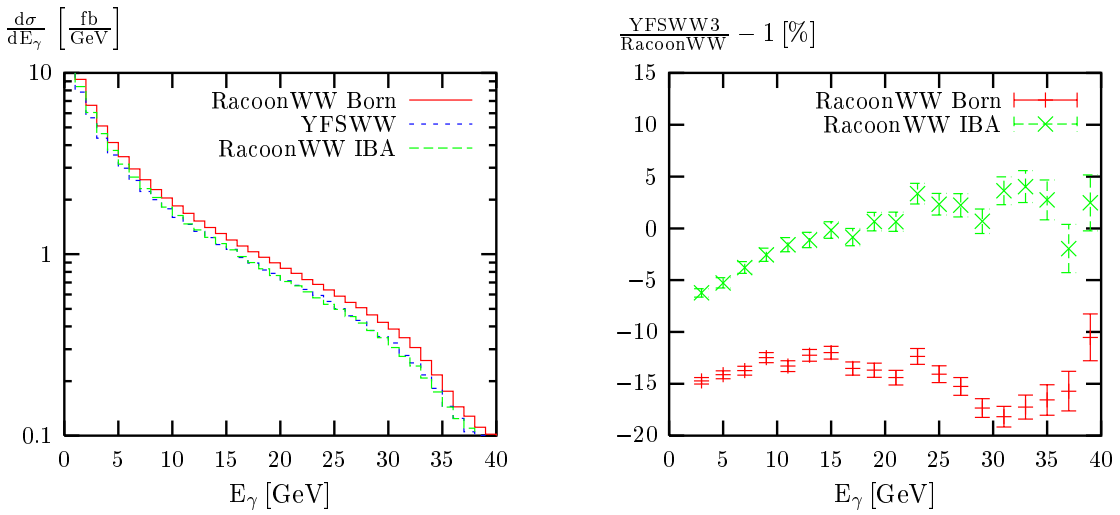

Figure 5: Distribution in the photon energy for the process $e^+e^- \to u\bar{d}\mu^-\bar{\nu}_\mu\gamma$ at $\sqrt{s} = 200\,\text{GeV}$

We restrict ourselves to the "bare" recombination scheme (see Refs. [8, 11] for details). Moreover, the W-boson width is calculated including the full $\mathcal{O}(\alpha)$ electroweak corrections together with naive QCD corrections resulting in $\Gamma_W = 2.08699\,\text{GeV}$. We compare the distributions in the photon energy E_γ, in the cosine of the polar angle θ_γ of the photon w.r.t. the e^+ beam, and in the angle $\theta_{\gamma f}$ between the photon and the nearest charged final-state fermion for the process $e^+e^- \to u\bar{d}\mu^-\bar{\nu}_\mu\gamma$ at $\sqrt{s} = 200\,\text{GeV}$. The differences of 15–20% between YFSWW3 and the pure Born prediction of RacoonWW (RacoonWW Born), which have already been shown in Ref. [11], reduce to about 5% once the leading logarithmic ISR corrections are included in RacoonWW (RacoonWW IBA). The remaining differences should be due to the still quite different treatment of visible photon radiation in RacoonWW and YFSWW3: in contrast to RacoonWW, YFSWW does not include the complete lowest-order matrix elements for $e^+e^- \to 4f\gamma$. Instead, the photon radiation from the final state is treated via PHOTOS [28]. In particular, for small photon energies, where the differences are largest, the non-factorizable contributions, which are not yet included in YFSWW3, might play a role.

In Figures 8–10 we extend the comparison of the photonic distributions between YFSWW3 and RacoonWW to 500 GeV. Here the difference is typically at the level of 10% and in general not reduced by the inclusion of ISR for $e^+e^- \to 4f\gamma$ in RacoonWW, i.e. the agreement without ISR in RacoonWW was accidentally good. One should also recall that the diagrams without two resonant W bosons (background diagrams) become more and more important at higher energies. Thus, the increasing difference between YFSWW3 and RacoonWW for higher energies could be due to a less efficient description of final-state radiation by the effective treatment with PHOTOS.

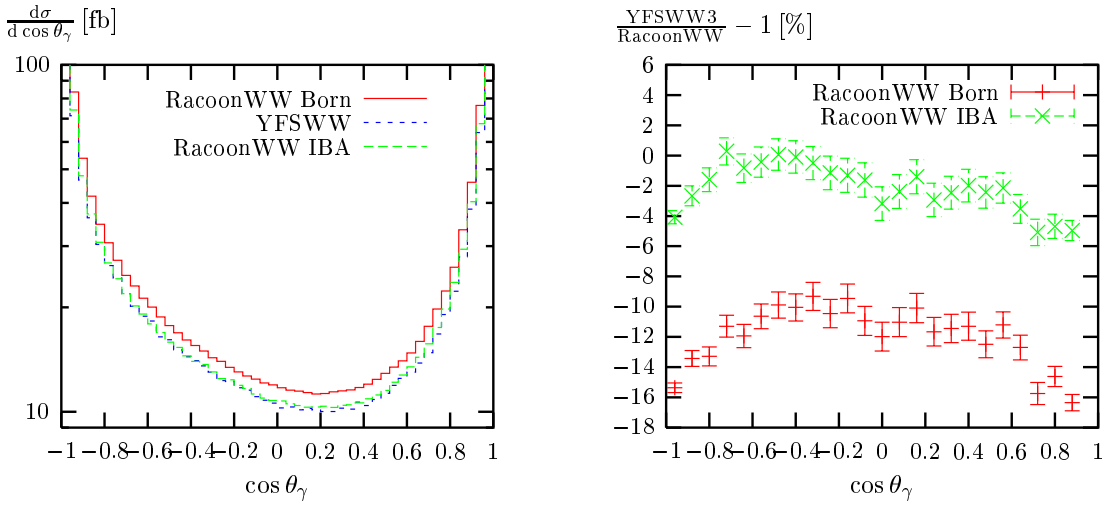

Figure 6: Distribution in the cosine of the polar angle of the photon w.r.t. the e^+ beam for the process $e^+e^- \to u\bar{d}\mu^-\bar{\nu}_\mu\gamma$ at $\sqrt{s} = 200\,\text{GeV}$

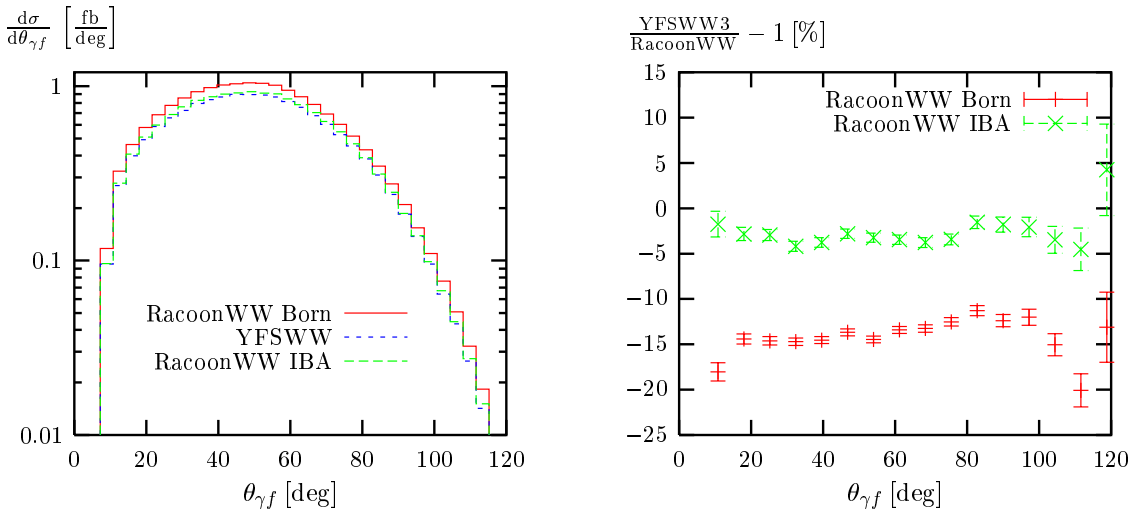

Figure 7: Distribution in the angle between the photon and the nearest charged final-state fermion for the process $e^+e^- \to u\bar{d}\mu^-\bar{\nu}_\mu\gamma$ at $\sqrt{s} = 200\,\text{GeV}$

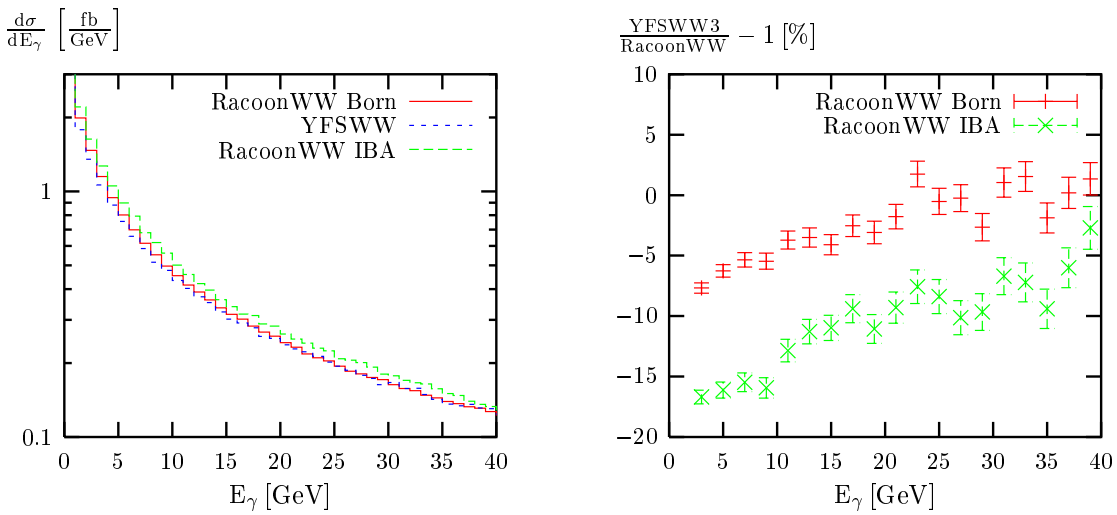

Figure 8: Distribution in the photon energy for the process $e^+e^- \to u\bar{d}\mu^-\bar{\nu}_\mu\gamma$ at $\sqrt{s} = 500\,\mathrm{GeV}$

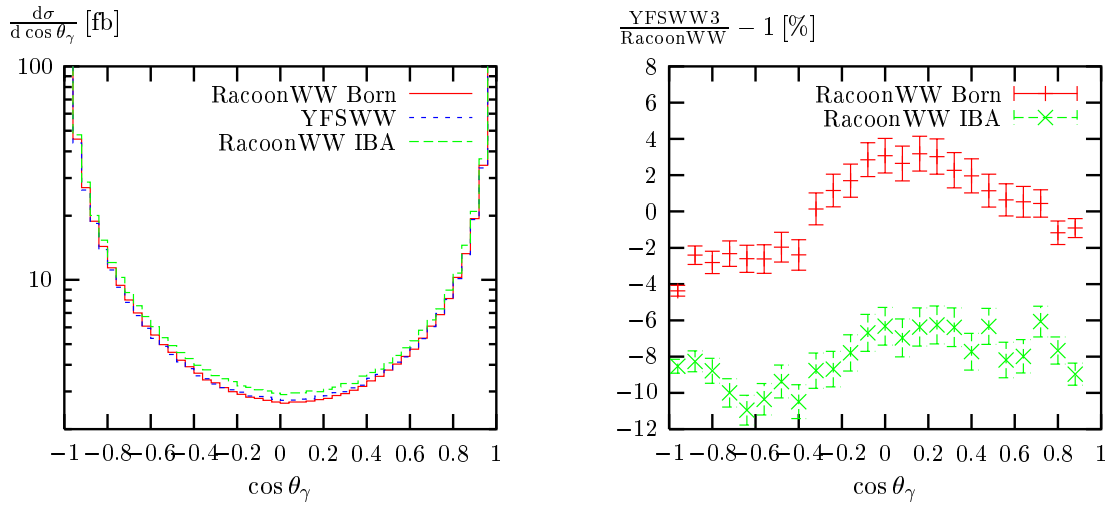

Figure 9: Distribution in the cosine of the polar angle of the photon w.r.t. the e^+ beam for the process $e^+e^- \to u\bar{d}\mu^-\bar{\nu}_\mu\gamma$ at $\sqrt{s} = 500\,\mathrm{GeV}$

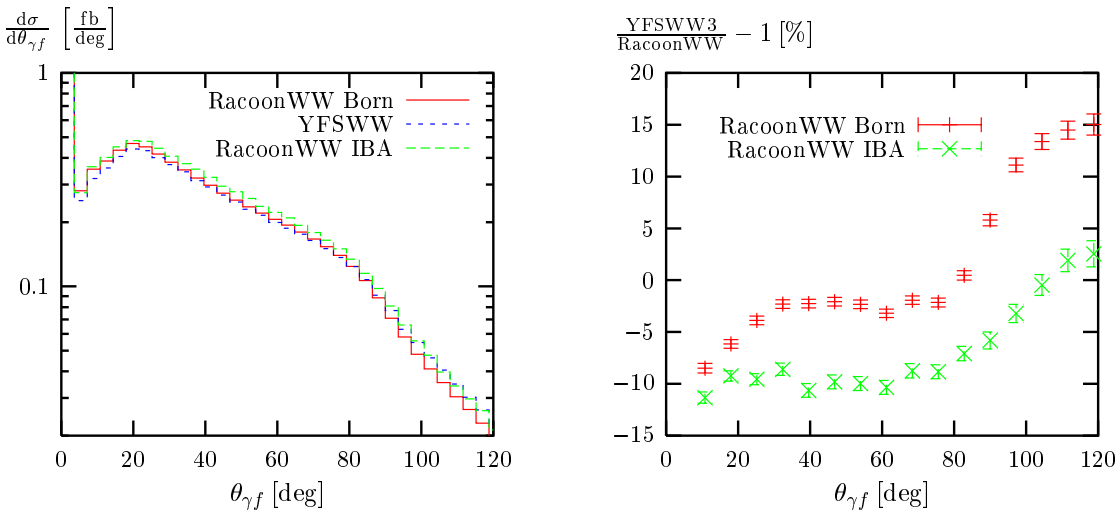

Figure 10: Distribution in the angle between the photon and the nearest charged final-state fermion for the process $e^+e^- \to u\bar{d}\mu^-\bar{\nu}_\mu\gamma$ at $\sqrt{s} = 500\,\mathrm{GeV}$

5.2 Standard Model predictions

We now discuss the predictions of RacoonWW for various observables in the SM. Here and in the following, the width is always calculated from the input parameters in lowest order in the G_μ scheme including naive QCD corrections ($\Gamma_W = 2.09436\,\mathrm{GeV}$). Naive QCD corrections are included in all results, in particular, also in the Born results.

The results in the LEP2 energy range were obtained with the ADLO/TH cuts as defined in Ref. [9], those at $\sqrt{s} = 500\,\mathrm{GeV}$ with the cuts

$$\begin{aligned}
\theta(l,\mathrm{beam}) &> 10^\circ, & \theta(l,l') &> 5^\circ, & \theta(l,q) &> 5^\circ,\\
\theta(\gamma,\mathrm{beam}) &> 1^\circ, & \theta(\gamma,l) &> 5^\circ, & \theta(\gamma,q) &> 5^\circ,\\
E_\gamma &> 0.1\,\mathrm{GeV}, & E_l &> 1\,\mathrm{GeV}, & E_q &> 3\,\mathrm{GeV},\\
m(q,q') &> 0.1\,\mathrm{GeV}, & \theta(q,\mathrm{beam}) &> 5^\circ, & &
\end{aligned} \tag{5.1}$$

where $\theta(i,j)$ specifies the angle between the particles i and j in the LAB system, and l, q, γ, and "beam" denote charged final-state leptons, quarks, photons, and the beam electrons or positrons, respectively. The invariant mass of a quark pair qq' is denoted by $m(q,q')$. The cuts (5.1) differ from the ADLO/TH cuts only in the looser cut on $m(q,q')$ and in the additional cut on $\theta(q,\mathrm{beam})$.

In Figure 11 we present the total cross section for the process $e^+e^- \to u\bar{d}\mu^-\bar{\nu}_\mu\gamma$ in the LEP2 energy range. On the left-hand side we show the absolute prediction in lowest order (Born), including ISR (ISR), and including in addition the Coulomb singularity according to variant 1) (IBA) discussed in Section 4. On the right-hand side we give the corrections relative to the lowest order including in addition a curve with the Coulomb singularity according to variant 2) (IBA2). The Coulomb singularity reaches about 5% at threshold and decreases with increasing energy. The effect is comparable to the one for the process without photon. The two variants for the implementation of the Coulomb

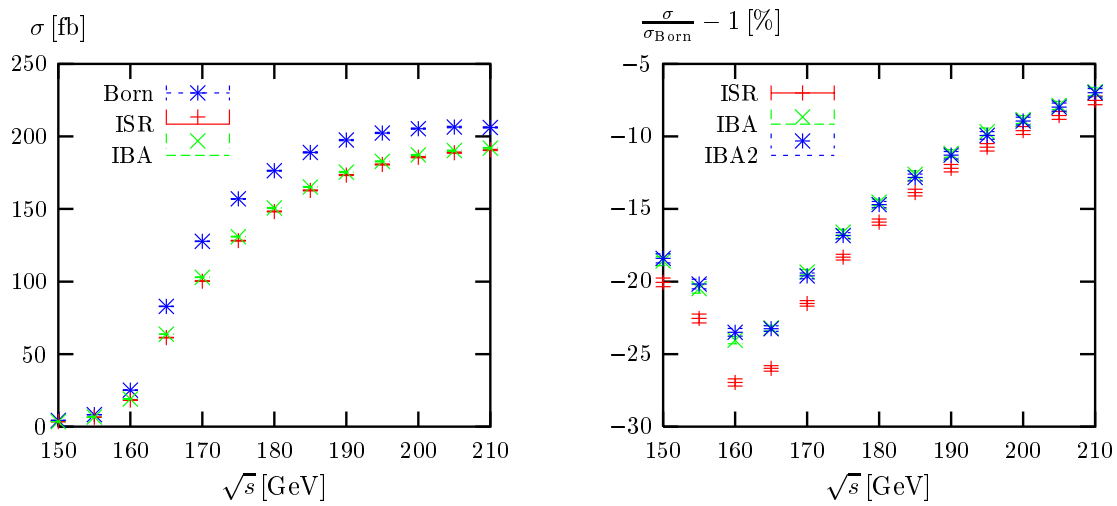

Figure 11: Total cross section for the process $e^+e^- \to u\bar{d}\mu^-\bar{\nu}_\mu\gamma$ as a function of the CM energy.

singularity show hardly any difference. Consequently, we will always use variant 1) in the following.

In Figures 12–14 we present the distributions in the photon energy E_γ, in the cosine of the polar angle θ_γ of the photon w.r.t. the e^+ beam, and in the angle $\theta_{\gamma f}$ between the photon and the nearest charged final-state fermion for $\sqrt{s} = 200\,\mathrm{GeV}$. The left-hand sides contain the absolute prediction for the process $e^+e^- \to u\bar{d}\mu^-\bar{\nu}_\mu\gamma$ in lowest order (Born) and including the ISR corrections and the Coulomb singularity (IBA), and for the process $e^+e^- \to u\bar{d}e^-\bar{\nu}_e\gamma$ including these corrections. The relative corrections (right-hand sides) are typically of the order of -10% wherever the cross sections are sizeable. Relative to the corresponding lowest-order results, the corrections to $e^+e^- \to u\bar{d}e^-\bar{\nu}_e\gamma$ would practically be indistinguishable from the relative corrections to $e^+e^- \to u\bar{d}\mu^-\bar{\nu}_\mu\gamma$. We therefore prefer to plot the corrections to $e^+e^- \to u\bar{d}e^-\bar{\nu}_e\gamma$ normalized to the lowest-order of $e^+e^- \to u\bar{d}\mu^-\bar{\nu}_\mu\gamma$ in order to visualize the effect of the "background" diagrams contained in $e^+e^- \to u\bar{d}e^-\bar{\nu}_e\gamma$. As can be seen, this effect is comparable to the radiative corrections but of opposite sign.

In Figures 15–17 we show results for $\sqrt{s} = 500\,\mathrm{GeV}$. Here, the left-hand sides contain the absolute prediction for the processes $e^+e^- \to u\bar{d}\mu^-\bar{\nu}_\mu\gamma$ and $e^+e^- \to u\bar{d}e^-\bar{\nu}_e\gamma$ in lowest order (Born) and including the ISR corrections and the Coulomb singularity (IBA). Note that here the distributions differ sizeably between the two processes. Therefore, on the right-hand sides, the IBA predictions for both processes are normalized to the corresponding lowest-order predictions. Where the cross sections are sizeable, the corrections are about $+10\%$ for $e^+e^- \to u\bar{d}\mu^-\bar{\nu}_\mu\gamma$ and $+5\%$ for $e^+e^- \to u\bar{d}e^-\bar{\nu}_e\gamma$. They are larger where the cross sections are small.

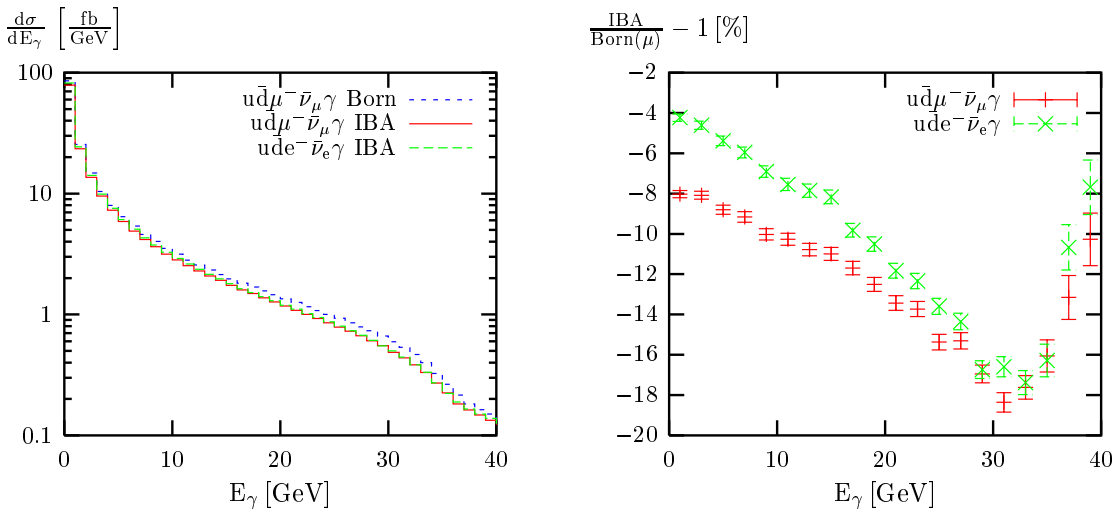

Figure 12: Distribution in the photon energy for the processes $e^+e^- \to u\bar{d}\mu^-\bar{\nu}_\mu\gamma$ and $e^+e^- \to u\bar{d}e^-\bar{\nu}_e\gamma$ at $\sqrt{s} = 200\,\text{GeV}$ ("Born(μ)" indicates that the Born cross section for $e^+e^- \to u\bar{d}\mu^-\bar{\nu}_\mu\gamma$ is taken.)

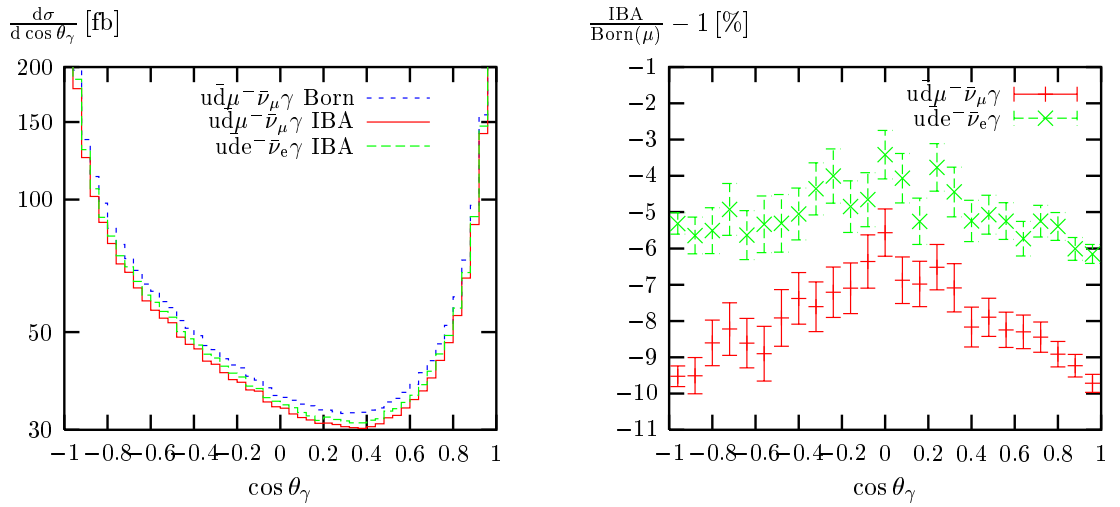

Figure 13: Distribution in the cosine of the polar angle of the photon w.r.t. the e^+ beam for the processes $e^+e^- \to u\bar{d}\mu^-\bar{\nu}_\mu\gamma$ and $e^+e^- \to u\bar{d}e^-\bar{\nu}_e\gamma$ at $\sqrt{s} = 200\,\text{GeV}$ ("Born(μ)" indicates that the Born cross section for $e^+e^- \to u\bar{d}\mu^-\bar{\nu}_\mu\gamma$ is taken.)

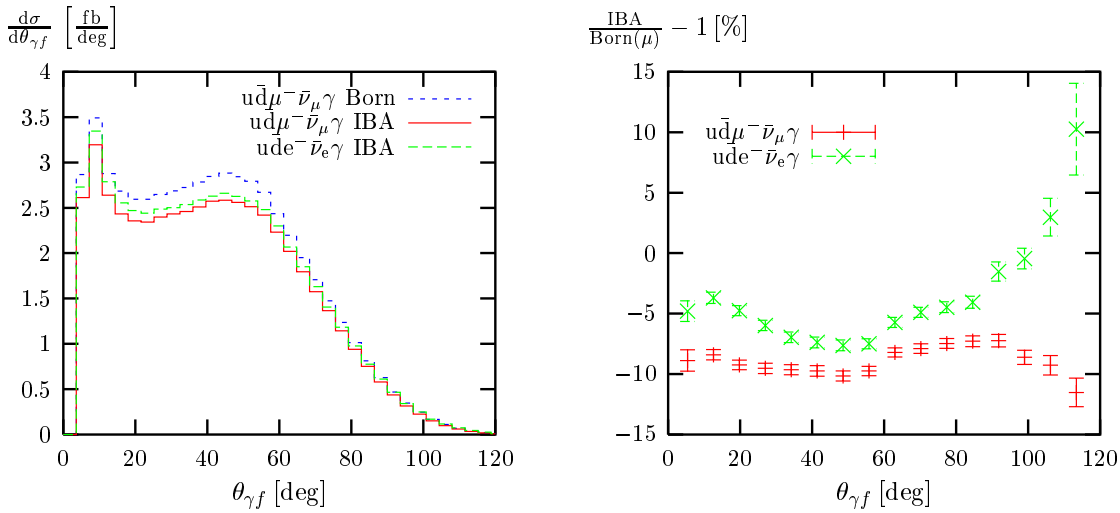

Figure 14: Distribution in the angle between the photon and the nearest charged final-state fermion for the processes $e^+e^- \to u\bar{d}\mu^-\bar{\nu}_\mu\gamma$ and $e^+e^- \to u\bar{d}e^-\bar{\nu}_e\gamma$ at $\sqrt{s} = 200\,\mathrm{GeV}$ ("Born(μ)" indicates that the Born cross section for $e^+e^- \to u\bar{d}\mu^-\bar{\nu}_\mu\gamma$ is taken.)

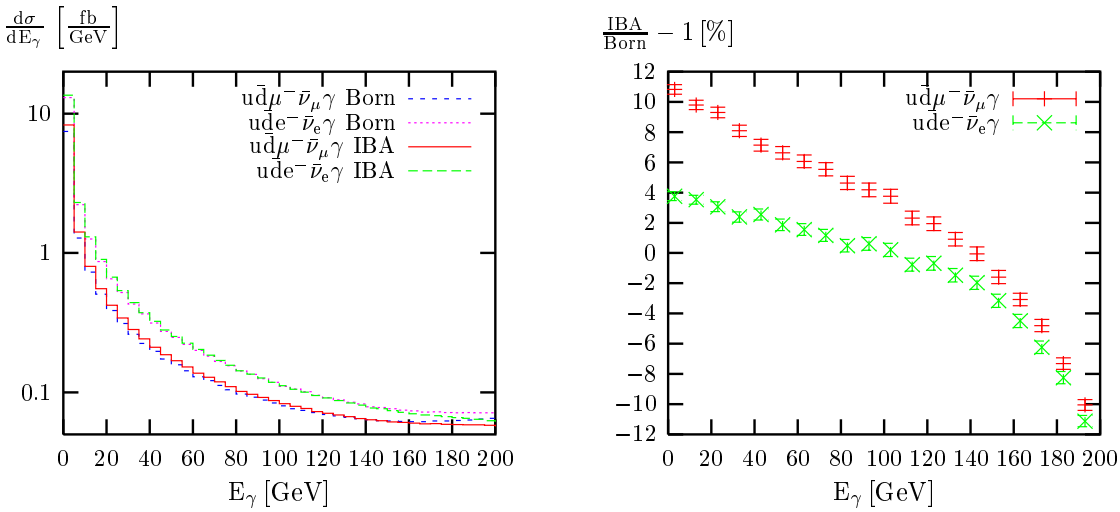

Figure 15: Distribution in the photon energy for the processes $e^+e^- \to u\bar{d}\mu^-\bar{\nu}_\mu\gamma$ and $e^+e^- \to u\bar{d}e^-\bar{\nu}_e\gamma$ at $\sqrt{s} = 500\,\mathrm{GeV}$

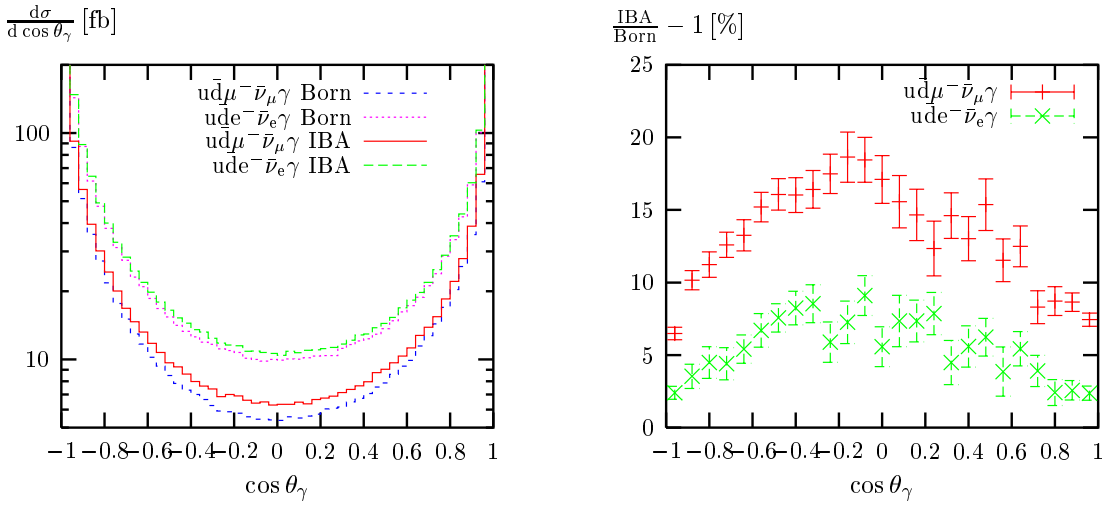

Figure 16: Distribution in the cosine of the polar angle of the photon w.r.t. the e^+ beam for the processes $e^+e^- \to u\bar{d}\mu^-\bar{\nu}_\mu\gamma$ and $e^+e^- \to u\bar{d}e^-\bar{\nu}_e\gamma$ at $\sqrt{s} = 500\,\text{GeV}$

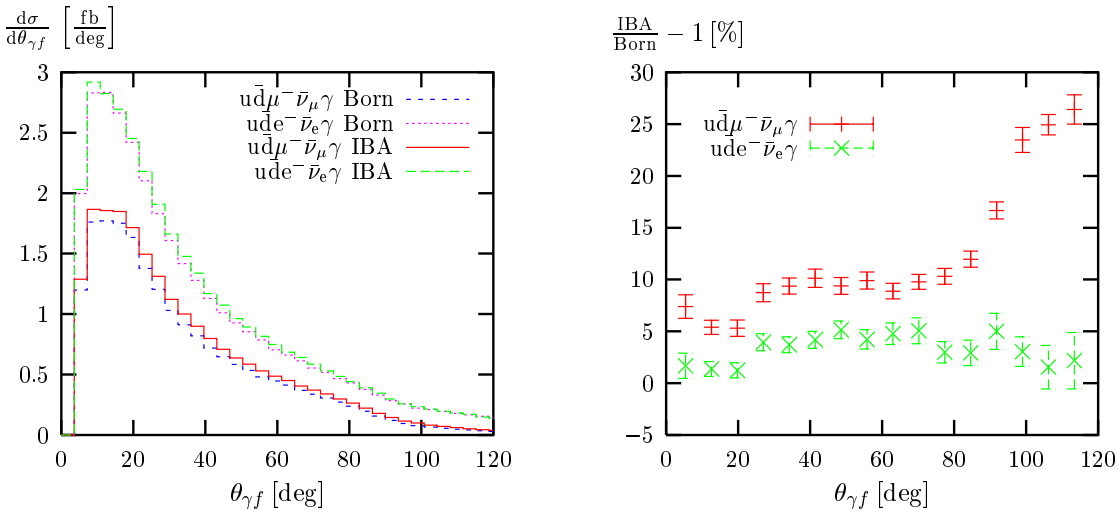

Figure 17: Distribution in the angle between the photon and the nearest charged final-state fermion for the processes $e^+e^- \to u\bar{d}\mu^-\bar{\nu}_\mu\gamma$ and $e^+e^- \to u\bar{d}e^-\bar{\nu}_e\gamma$ at $\sqrt{s} = 500\,\text{GeV}$

5.3 Predictions with anomalous quartic couplings

Since the matrix element depends linearly on the anomalous quartic couplings a_i, the cross section is a quadratic form in the a_i. Therefore, it is sufficient to evaluate the cross section for a finite set of sample values of the anomalous quartic couplings in order to get the cross section for arbitrary values of these couplings. We restrict ourselves here to the semileptonic process $e^+e^- \to u\bar{d}\mu^-\bar{\nu}_\mu\gamma$ and include ISR and the Coulomb singularity (variant 1). We use the cuts

$$E_\gamma > 5\,\mathrm{GeV}, \qquad |\cos\theta_\gamma| < 0.95, \qquad |\cos\theta_{\gamma f}| < 0.90, \qquad m(f,f') = M_\mathrm{W} \pm 2\Gamma_\mathrm{W}, \tag{5.2}$$

where E_γ is the energy of the photon, θ_γ the angle between the photon and the beam axis, $\theta_{\gamma f}$ the angle between the photon and any charged final-state fermion f, and $m(f,f')$ the invariant mass of the fermion–antifermion pairs that result from W decay. In the computation of $m(\mu,\nu_\mu)$ the momentum of the neutrino is set equal to the missing momentum, since the neutrino is not detected, i.e. the energy loss in the ISR convolution (4.2) is implicitly included in the neutrino momentum.

We first study the influence of the AQGC a_0, a_c, a_n, $\tilde{a}_0$, and $\tilde{a}_\mathrm{n}$ on the cross section at $\sqrt{s} = 200\,\mathrm{GeV}$ and $500\,\mathrm{GeV}$ separately. Figure 18 shows the cross section normalized to the SM value as a function of each of these couplings for all the other a_i's equal to zero. The asymmetry results from the interference between the SM matrix element and the matrix element of the AQGC, which is suppressed for the CP-violating couplings a_n and $\tilde{a}_0$. The asymmetry is small for a_0 and $\tilde{a}_\mathrm{n}$ and only visible at $\sqrt{s} = 500\,\mathrm{GeV}$ for a_0 in Figure 18, but sizeable for a_c.[4] The cross section is most sensitive to a_0 and $\tilde{a}_0$ and least sensitive to a_n and $\tilde{a}_\mathrm{n}$.

In order to illustrate the potential of LEP2 and a linear e^+e^- collider in putting limits on the AQGC, we consider the following two scenarios: an integrated luminosity $\mathcal{L} = 320\,\mathrm{pb}^{-1}$ at $\sqrt{s} = 200\,\mathrm{GeV}$ and $\mathcal{L} = 50\,\mathrm{fb}^{-1}$ at $\sqrt{s} = 500\,\mathrm{GeV}$. The corresponding total SM cross sections to $e^+e^- \to u\bar{d}\mu^-\bar{\nu}_\mu\gamma$ are 16.69 fb and 7.64 fb, respectively. Assuming that the measured number N of events is given by the SM cross section $\sigma_\mathrm{SM} = \sigma(a_i = 0)$ and the experimental errors by the corresponding square-root, we define

$$\chi^2 \equiv \frac{(N(a_i) - N)^2}{N} = \left(\frac{\sigma(a_i)}{\sigma_\mathrm{SM}} - 1\right)^2 \sigma_\mathrm{SM}\mathcal{L}, \tag{5.3}$$

where $N(a_i)$ is the number of events that result from the cross section with anomalous couplings. Since the square-root of this χ^2 distribution is a quadratic form in the a_i, the hypersurfaces of constant χ^2 form ellipsoids. The 1σ limits resulting from $\chi^2 = 1$ on individual couplings can be illustrated by projecting the ellipsoids into the planes corresponding to pairs of couplings. Instead of the projections, often the sections of the planes with the ellipsoids are used. Note that the ellipses resulting from projections are in general larger and include those ellipses resulting from sections of the planes with the ellipsoids. Since the correlations are small for the cases under consideration, the difference

[4] The sign of the asymmetry differs from the results of Ref. [7], since the couplings a_0 and a_c have been implemented [29] in EEWWG with a sign opposite to the definitions in Refs. [7, 17], which agree with our choice.

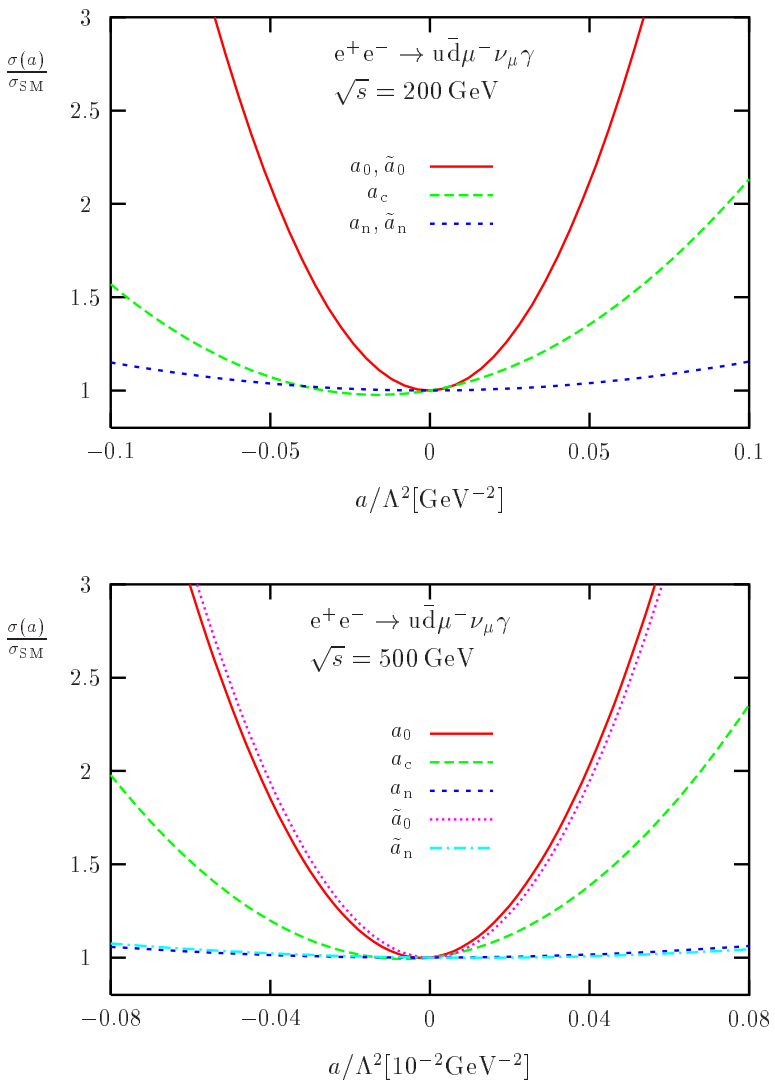

Figure 18: Impact of the AQGC a_0, a_c, a_n, $\tilde{a}_0$, and $\tilde{a}_n$ on the cross section for $e^+e^- \to u\bar{d}\mu^-\bar{\nu}_\mu\gamma$ at $\sqrt{s} = 200\,\mathrm{GeV}$ and $500\,\mathrm{GeV}$. Only one of the AQGC a_i is varied while the others are kept zero.

between both types of ellipses is also small. In the following figures we include both the projections and the sections of the ellipsoids using the same type of lines.

In Figures 19 and 20 we show some 1σ contours for various pairs of a_i. In addition we list the 1σ limits derived from projecting the ellipsoids. Since the effects of a_0 and $\tilde{a}_0$ and of a_n and $\tilde{a}_\mathrm{n}$ on the cross section are equal up to relatively small interference terms, also the corresponding contours of these couplings with other couplings are of similar size. For transparency we omitted some contours involving a_n; for 200 GeV (Figure 19) these contours practically coincide with the ones for $\tilde{a}_\mathrm{n}$, for 500 GeV (Figure 20) the contours for a_n are of the same size and shape as the ones for $\tilde{a}_\mathrm{n}$ but shifted to become approximately symmetric w.r.t. $a_\mathrm{n} \to -a_\mathrm{n}$. The best limits can be obtained for a_0 and $\tilde{a}_0$. The correlations between the different couplings are in general small, and only a_0 and a_c show a noticeable correlation. The limits obtainable at a linear collider are by about a factor of 200 better than those obtainable at LEP2. This improvement reflects the enhanced sensitivity of the cross section on the anomalous couplings at high energies, which can also be seen in Figure 18, and to a smaller part the higher luminosity.

6 Summary

We have calculated all lowest-order amplitudes for $\mathrm{e^+e^-} \to 4f\gamma$ with five different genuine anomalous quartic gauge-boson couplings that are allowed by electromagnetic gauge invariance and the custodial $\mathrm{SU(2)_c}$ symmetry. These couplings include the three operators $\mathcal{L}_0$, $\mathcal{L}_\mathrm{c}$, and $\mathcal{L}_\mathrm{n}$, which have been constrained by the LEP collaborations by analysing $\mathrm{WW}\gamma$ production, and two additional P-violating couplings, one of which conserves CP. The five anomalous couplings have been incorporated in the $4f(\gamma)$ Monte Carlo generator RacoonWW. We have calculated the dependence of the cross section for $\mathrm{e^+e^-} \to 4f\gamma$ on the anomalous quartic couplings and illustrated the typical size of the limits that can be obtained for these couplings at LEP2 and a 500 GeV $\mathrm{e^+e^-}$ collider.

Moreover, we have implemented the dominant leading electroweak corrections to $\mathrm{e^+e^-} \to 4f\gamma$ into RacoonWW. These include initial-state radiation, the dominant universal effects originating from the running of the couplings, and the Coulomb singularity for processes involving W-boson pairs. We have compared the corresponding predictions with existing calculations, as far as possible, and investigated the numerical impact of the dominant corrections.

With the additions described in this paper, RacoonWW is a state-of-the-art Monte Carlo generator for the classes of $\mathrm{e^+e^-} \to 4f$ and $\mathrm{e^+e^-} \to 4f\gamma$ processes with arbitrary massless four-fermion final states, both for the Standard Model and including anomalous quartic gauge-boson couplings.

Acknowledgement

We are grateful to U. Parzefall and M. Thomson for providing us with suitable experimental cuts for AQGC studies. Moreover, we thank A. Werthenbach for discussions about Refs. [7, 17] and for making the program EEWWG available to us. Finally, we thank the WRAP and YFSWW3 teams for their collaboration in preparing the comparisons with their results.

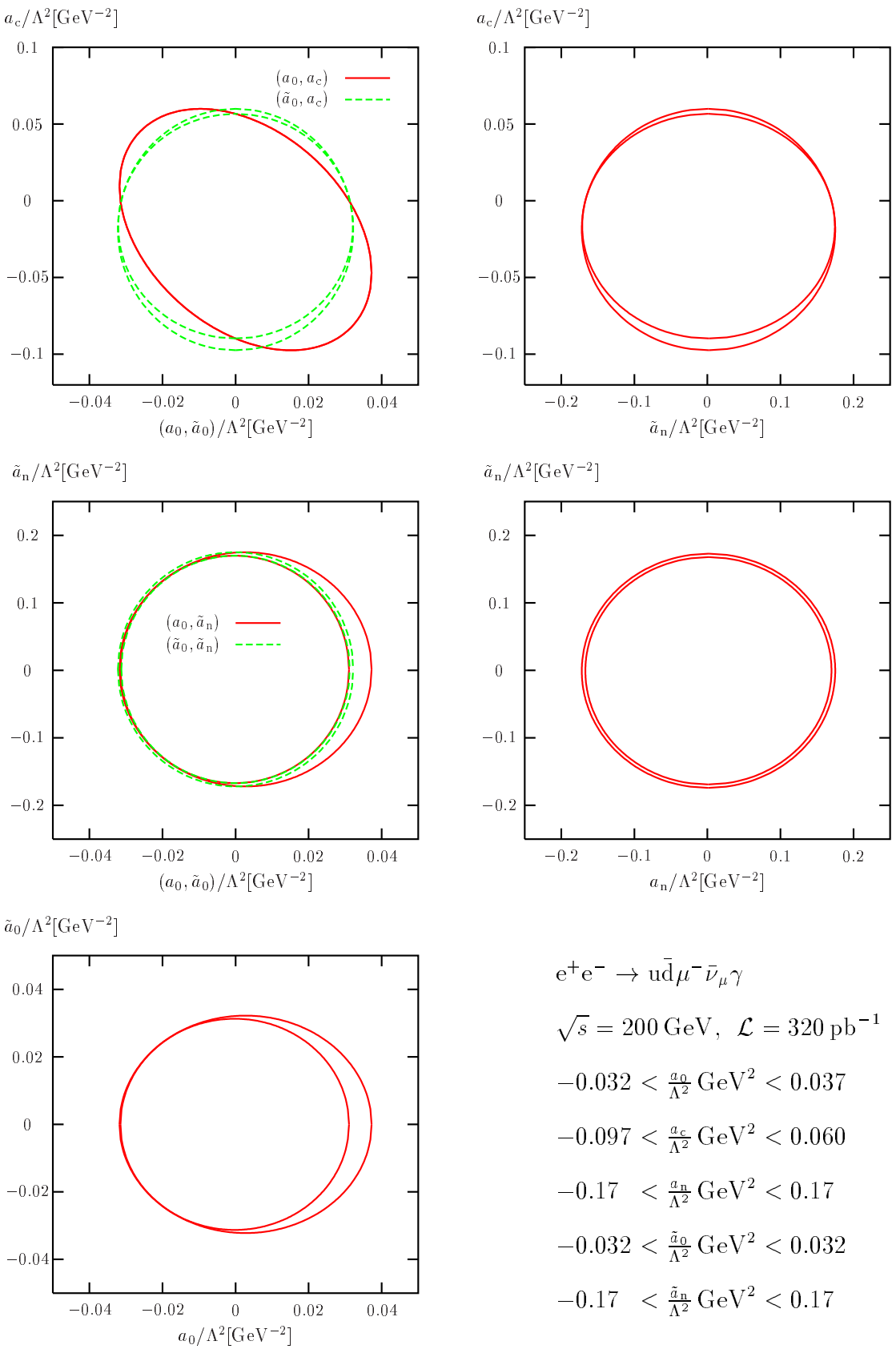

$$e^+e^- \to u\bar{d}\mu^-\bar{\nu}_\mu\gamma$$

$$\sqrt{s} = 200\,\mathrm{GeV}, \quad \mathcal{L} = 320\,\mathrm{pb}^{-1}$$

$$-0.032 < \tfrac{a_0}{\Lambda^2}\,\mathrm{GeV}^2 < 0.037$$

$$-0.097 < \tfrac{a_c}{\Lambda^2}\,\mathrm{GeV}^2 < 0.060$$

$$-0.17 < \tfrac{a_n}{\Lambda^2}\,\mathrm{GeV}^2 < 0.17$$

$$-0.032 < \tfrac{\tilde{a}_0}{\Lambda^2}\,\mathrm{GeV}^2 < 0.032$$

$$-0.17 < \tfrac{\tilde{a}_n}{\Lambda^2}\,\mathrm{GeV}^2 < 0.17$$

Figure 19: 1σ contours in various (a_i, a_j) planes for the process $e^+e^- \to u\bar{d}\mu^-\bar{\nu}_\mu\gamma$ at $\sqrt{s} = 200\,\mathrm{GeV}$

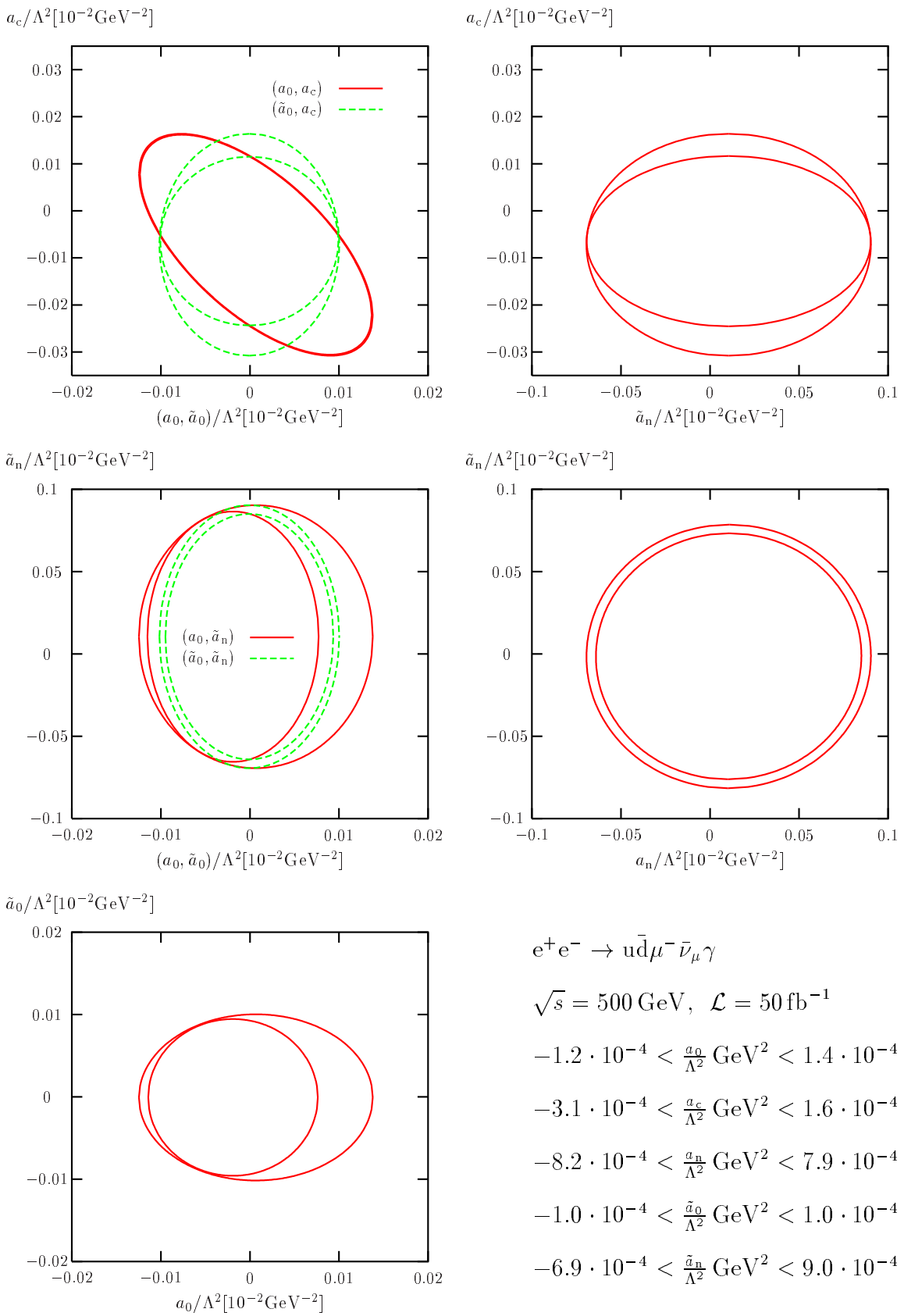

$$e^+e^- \to u\bar{d}\mu^-\bar{\nu}_\mu\gamma$$

$$\sqrt{s} = 500\,\mathrm{GeV}, \quad \mathcal{L} = 50\,\mathrm{fb}^{-1}$$

$$-1.2 \cdot 10^{-4} < \frac{a_0}{\Lambda^2}\,\mathrm{GeV}^2 < 1.4 \cdot 10^{-4}$$

$$-3.1 \cdot 10^{-4} < \frac{a_c}{\Lambda^2}\,\mathrm{GeV}^2 < 1.6 \cdot 10^{-4}$$

$$-8.2 \cdot 10^{-4} < \frac{a_n}{\Lambda^2}\,\mathrm{GeV}^2 < 7.9 \cdot 10^{-4}$$

$$-1.0 \cdot 10^{-4} < \frac{\tilde{a}_0}{\Lambda^2}\,\mathrm{GeV}^2 < 1.0 \cdot 10^{-4}$$

$$-6.9 \cdot 10^{-4} < \frac{\tilde{a}_n}{\Lambda^2}\,\mathrm{GeV}^2 < 9.0 \cdot 10^{-4}$$

Figure 20: 1σ contours in various (a_i, a_j) planes for the process $e^+e^- \to u\bar{d}\mu^-\bar{\nu}_\mu\gamma$ at $\sqrt{s} = 500\,\mathrm{GeV}$

This work was supported in part by the Swiss Bundesamt für Bildung und Wissenschaft, by the European Union under contract HPRN-CT-2000-00149, by the U.S. Department of Energy under grant DE-FG02-91ER40685 and by the U.S. National Science Foundation under grant PHY-9600155.

Appendix

A Some corrections to the generic construction of $e^+e^- \to 4f\gamma$ amplitudes

In Ref. [9] we have constructed the amplitudes for all $e^+e^- \to 4f\gamma$ reactions from the two basic channels CCa and NCa, which are also specified in Section 3. Here we take the opportunity to correct two mistakes in the corresponding formulas:

- Equation (2.24) of Ref. [9] is only correct for down-type fermions f, while some arguments have to be interchanged for up-type fermions. The correct formula is

$$\mathcal{M}^{\sigma_+,\sigma_-,\sigma_1,\sigma_2,\sigma_3,\sigma_4}_{\mathrm{CC/NCb}}(p_+,p_-,k_1,k_2,k_3,k_4)$$
$$= \begin{cases} \mathcal{M}^{\sigma_+,\sigma_-,\sigma_1,\sigma_2,\sigma_3,\sigma_4}_{\mathrm{NCa}}(p_+,p_-,k_1,k_2,k_3,k_4) \\ -\mathcal{M}^{-\sigma_3,-\sigma_4,\sigma_1,-\sigma_-,-\sigma_+,\sigma_2}_{\mathrm{CCa}}(-k_3,-k_4,k_1,-p_-,-p_+,k_2) \quad \text{for } I^3_{\mathrm{w},f} = -1/2, \\ \\ \mathcal{M}^{\sigma_+,\sigma_-,\sigma_1,\sigma_2,\sigma_3,\sigma_4}_{\mathrm{NCa}}(p_+,p_-,k_1,k_2,k_3,k_4) \\ -\mathcal{M}^{-\sigma_3,-\sigma_4,-\sigma_+,\sigma_2,\sigma_1,-\sigma_-}_{\mathrm{CCa}}(-k_3,-k_4,-p_+,k_2,k_1,-p_-) \quad \text{for } I^3_{\mathrm{w},f} = +1/2. \end{cases} \tag{A.1}$$

  The error affected the evaluation of the final states $\nu_e\bar{\nu}_e\nu_\mu\bar{\nu}_\mu$ and $\nu_e\bar{\nu}_e u\bar{u}$ in Table 1 of Ref. [9] at the level of 0.2–0.4%. The corrected results for Table 1 are

σ/fb	$e^+e^- \to 4f$ running width	$e^+e^- \to 4f$ constant width	$e^+e^- \to 4f\gamma$ constant width
$\nu_e\bar{\nu}_e\nu_\mu\bar{\nu}_\mu$	8.339(2)	8.321(2)	1.511(1)
$\nu_e\bar{\nu}_e u\,\bar{u}$	23.91(2)	23.90(2)	6.79(3)

  For the final states $\nu_e\bar{\nu}_e\nu_\mu\bar{\nu}_\mu\gamma$ and $\nu_e\bar{\nu}_e u\bar{u}\gamma$ no change is visible in the numerical results within the integration errors after the correction. The numerical smallness of the correction is due to the fact that the two cases in (A.1) differ only in the contribution of a non-resonant background diagram which is suppressed.

- Equation (2.25) of Ref. [9] contains some misprints. The correct formula is

$$\begin{aligned} &\mathcal{M}^{\sigma_+,\sigma_-,\sigma_1,\sigma_2,\sigma_3,\sigma_4}_{\mathrm{CC/NCc}}(p_+,p_-,k_1,k_2,k_3,k_4) \\ &\quad = \quad \mathcal{M}^{\sigma_+,\sigma_-,\sigma_1,\sigma_2,\sigma_3,\sigma_4}_{\mathrm{NCa}}(p_+,p_-,k_1,k_2,k_3,k_4) \\ &\qquad - \mathcal{M}^{\sigma_+,\sigma_-,\sigma_3,\sigma_2,\sigma_1,\sigma_4}_{\mathrm{NCa}}(p_+,p_-,k_3,k_2,k_1,k_4) \\ &\qquad - \mathcal{M}^{-\sigma_1,-\sigma_2,-\sigma_+,\sigma_4,\sigma_3,-\sigma_-}_{\mathrm{CCa}}(-k_1,-k_2,-p_+,k_4,k_3,-p_-) \\ &\qquad + \mathcal{M}^{-\sigma_1,-\sigma_4,-\sigma_+,\sigma_2,\sigma_3,-\sigma_-}_{\mathrm{CCa}}(-k_1,-k_4,-p_+,k_2,k_3,-p_-) \\ &\qquad + \mathcal{M}^{-\sigma_3,-\sigma_2,-\sigma_+,\sigma_4,\sigma_1,-\sigma_-}_{\mathrm{CCa}}(-k_3,-k_2,-p_+,k_4,k_1,-p_-) \\ &\qquad - \mathcal{M}^{-\sigma_3,-\sigma_4,-\sigma_+,\sigma_2,\sigma_1,-\sigma_-}_{\mathrm{CCa}}(-k_3,-k_4,-p_+,k_2,k_1,-p_-). \end{aligned} \tag{A.2}$$

However, the numerical evaluations for the corresponding $\nu_e\bar{\nu}_e\nu_e\bar{\nu}_e(\gamma)$ final states were based on this correct form.

References

[1] T. Barklow and K. McFarland, talks given at the *5th International Symposium on Radiative Corrections (RADCOR–2000)*, Carmel CA, USA, 2000.

[2] G. Abbiendi *et al.* [OPAL Collaboration], Phys. Lett. B **471** (1999) 293 [hep-ex/9910069].

[3] M. Acciarri *et al.* [L3 Collaboration], Phys. Lett. B **490** (2000) 187 [hep-ex/0008022].

[4] The LEP Collaborations ALEPH, DELPHI, L3, OPAL, the LEP Electroweak Working Group, and the SLD Heavy Flavour and Electroweak Groups, CERN-EP/2001-021, hep-ex/0103048.

[5] G. Gounaris *et al.*, in *Physics at LEP2*, eds. G. Altarelli, T. Sjöstrand and F. Zwirner (CERN 96-01, Geneva, 1996), Vol. 1, p. 525 [hep-ph/9601233].

[6] G. Montagna, M. Moretti, O. Nicrosini, M. Osmo and F. Piccinini, hep-ph/0103155.

[7] W. J. Stirling and A. Werthenbach, Eur. Phys. J. C **14** (2000) 103 [hep-ph/9903315].

[8] A. Denner, S. Dittmaier, M. Roth and D. Wackeroth, Nucl. Phys. B **587** (2000) 67 [hep-ph/0006307].

[9] A. Denner, S. Dittmaier, M. Roth and D. Wackeroth, Nucl. Phys. B **560** (1999) 33 [hep-ph/9904472].

[10] J. Fujimoto, T. Ishikawa, S. Kawabata, Y. Kurihara, Y. Shimizu and D. Perret-Gallix, Nucl. Phys. Proc. Suppl. **37B** (1994) 169 [hep-ph/9407308];
F. Caravaglios and M. Moretti, Z. Phys. C **74** (1997) 291 [hep-ph/9604316];
F. Jegerlehner and K. Kolodziej, Eur. Phys. J. C **12** (2000) 77 [hep-ph/9907229] and hep-ph/0012250;
C. G. Papadopoulos, hep-ph/0007335;
A. Kanaki and C. G. Papadopoulos, hep-ph/0012004.

[11] M. W. Grünewald *et al.*, in *Reports of the Working Groups on Precision Calculations for LEP2 Physics*, eds. S. Jadach, G. Passarino and R. Pittau (CERN 2000-009, Geneva, 2000), p. 1 [hep-ph/0005309].

[12] E. A. Kuraev and V. S. Fadin, *Yad. Fiz.* **41** (1985) 753 [*Sov. J. Nucl. Phys.* **41** (1985) 466];
G. Altarelli and G. Martinelli, in *"Physics at LEP"*, eds. J. Ellis and R. Peccei, CERN 86-02 (CERN, Geneva, 1986), Vol. 1, p. 47;
O. Nicrosini and L. Trentadue, Phys. Lett. B **196** (1987) 551; Z. Phys. C **39** (1988) 479;
F. A. Berends, W. L. van Neerven and G. J. Burgers, Nucl. Phys. B **297** (1988) 429; Erratum-ibid. B **304** (1988) 921.

[13] V. S. Fadin, V. A. Khoze and A. D. Martin, Phys. Lett. B **311** (1993) 311;
D. Bardin, W. Beenakker and A. Denner, Phys. Lett. B **317** (1993) 213;
V. S. Fadin, V. A. Khoze, A. D. Martin and A. Chapovsky, Phys. Rev. D **52** (1995) 1377 [hep-ph/9501214].

[14] P. Sikivie, L. Susskind, M. Voloshin and V. Zakharov, Nucl. Phys. B **173** (1980) 189.

[15] G. Bélanger and F. Boudjema, Phys. Lett. B **288** (1992) 201.

[16] G. Abu Leil and W. J. Stirling, J. Phys. G**21** (1995) 517 [hep-ph/9406317].

[17] W. J. Stirling and A. Werthenbach, Eur. Phys. J. C **12** (2000) 441 [hep-ph/9905341].

[18] G. Bélanger, F. Boudjema, Y. Kurihara, D. Perret-Gallix and A. Semenov, Eur. Phys. J. C **13** (2000) 283 [hep-ph/9908254].

[19] K. Hagiwara, R. D. Peccei, D. Zeppenfeld and K. Hikasa, Nucl. Phys. B **282** (1987) 253.

[20] S. Dittmaier, Phys. Rev. D **59** (1999) 016007 [hep-ph/9805445].

[21] M. Böhm, H. Spiesberger and W. Hollik, Fortsch. Phys. **34** (1986) 687;
A. Denner, Fortsch. Phys. **41** (1993) 307;
A. Denner, S. Dittmaier and G. Weiglein, Nucl. Phys. B **440** (1995) 95 [hep-ph/9410338].

[22] T. Stelzer and W. F. Long, Comput. Phys. Commun. **81** (1994) 357 [hep-ph/9401258];
H. Murayama, I. Watanabe and K. Hagiwara, KEK-91-11.

[23] A. Denner, S. Dittmaier, M. Roth and D. Wackeroth, hep-ph/0101257.

[24] W. Beenakker *et al.*, in *Physics at LEP2*, eds. G. Altarelli, T. Sjöstrand and F. Zwirner (CERN 96-01, Geneva, 1996), Vol. 1, p. 79 [hep-ph/9602351].

[25] A. Denner, S. Dittmaier and M. Roth, Nucl. Phys. B **519** (1998) 39 [hep-ph/9710521].

[26] G. Montagna, M. Moretti, O. Nicrosini and F. Piccinini, Nucl. Phys. B **541** (1999) 31 [hep-ph/9807465].

[27] S. Jadach, W. Placzek, M. Skrzypek, B. F. Ward and Z. Was, Phys. Lett. B **417** (1998) 326 [hep-ph/9705429]; Phys. Rev. D **61** (2000) 113010 [hep-ph/9907436]; hep-ph/0007012 and hep-ph/0103163.

[28] E. Barberio, B. van Eijk and Z. Was, Comput. Phys. Commun. **66** (1991) 115.

[29] A. Werthenbach, private communication.